

Design of fMRI-compatible electronic musical interfaces

Avrum Hollinger



Music Technology Area
Schulich School of Music
McGill University
Montreal, Canada

June 16, 2008

A thesis submitted to McGill University in partial fulfillment of the requirements for the
degree of Master of Arts.

© 2008 Avrum Hollinger

Abstract

The designs of two functional magnetic resonance imaging-compatible electronic interfaces for use in neuropsychological studies involving musical tasks are presented. The devices, a two-button response box in the form of a computer mouse and a piano keyboard, were designed for rhythmic tapping and piano performance tasks, respectively. In order to correlate changes in neural activation acquired through magnetic resonance imaging (MRI) with task performance, the electronic collection of behavioural data, such as the timing of button or key presses was required. These behavioural measures were captured electronically and communicated to a host computer for synchronization with feedback, stimuli, and the MRI scanner itself. As well, data was logged for offline analysis. Due to the intense and volatile electromagnetic fields, most commercially-available electronic interfaces do not function properly and can even pose a serious safety hazard within the MRI scanner environment. Therefore these custom-designed interfaces were free of ferromagnetic parts and all electronic components were relegated to the control room outside of the scanner environment. Acquisition of button and key presses was accomplished using fibre optic sensors, which are immune to electromagnetic interference. The devices performed successfully within the scanner, and MRI scans showed no image artifacts caused by the prototypes. Sensing of key and button transition velocity was sufficient after extensive calibration. Next generation prototypes are planned and will implement more robust and tighter tolerance manufacturing, improved sensing techniques, the acquisition of isometric forces, and an auto-calibration scheme.

Résumé

La conception de deux interfaces électroniques pour tâches musicales compatibles avec un appareil d'imagerie par résonance magnétique (IRM) fonctionnelle sont présentés. Les dispositifs, une interface à deux boutons ressemblant à une souris d'ordinateur et un clavier du piano, ont été utilisés respectivement lors de tâches de battues rythmiques et de jeu au piano dans le cadre d'études neuropsychologiques sur des musiciens. Elles ont permis de mesurer certaines données telles que les instants auxquels un bouton ou une touche ont été enfoncés et relâchée. Ces données ont été ensuite communiquées à un serveur permettant leur synchronisation avec les stimuli, les retours sonores, et l'appareil d'IRM. Elles ont aussi été enregistré en vue de traitements en temps différé. L'environnement d'IRM présente des difficultés et dangers, bien particuliers, du à l'intensité des champs électromagnétiques émis. Ces champs sont tellement puissants et changeants que les systèmes électroniques ne peuvent pas fonctionner. C'est pourquoi ces interfaces furent construites sans matériaux ferromagnétiques, et que toutes les pièces électroniques furent déplacées dans une salle de contrôle, hors de l'environnement d'IRM. L'acquisition des transitions de touches est donc assurée par des capteurs à fibres optiques, afin qu'elle soit insensible aux interférences électromagnétiques produites par l'appareil d'IRM. Grâce à ces précautions, les interfaces ont fonctionné correctement dans l'appareil d'IRM, et n'ont pas dégradé les images. À l'issu d'un long processus de calibration, le dispositif a permis de fournir des mesures de la vitesse de l'enfoncement des touches. De futures prototypes sont prévus et apporteront des améliorations au niveau de la manufacture, des systèmes d'acquisition, ainsi qu'un dispositif de calibration automatique.

Acknowledgments

A thank you to my supervisor, Marcelo Wanderley, for your guidance, assistance, and support from the very start. Your encouragement and enthusiasm surrounding my work and this project are much appreciated. Thank you Virginia Penhune and Robert Zatorre, the lead investigators of this project, for this amazing opportunity. I have thoroughly enjoyed working with you on this project and look forward to continuing this endeavour. Special thanks to Christopher Steele, who did much work to get all the scanning done, for your patience and insight, and for many a conversation whenever was needed. Many thanks to Allan Hollinger for many extended technical discussions and explanations, and to the rest of the family for sitting through some of it. Thank you to Alexander Koujelev at the Canadian Space Agency for our discussions on fibre optic sensing; to Louis Lovsin at Montreal Piano for donating the piano parts; to Brian Hynes of Hybex Innovations Inc. for our meetings regarding the scanner interface fixture; and to James Louder for sharing with me your experience on instrument building. To Michael Ferreira and the crew at the MNI, thank you for making sure things ran safely and smoothly during scanning sessions at the Neuro. Thanks to my professors and colleagues at the Music Tech lab for their assistance and feedback, with a special thanks to Stephen Sinclair for his help with typesetting, as well as Alexandre, Bertrand, Darryl, Doug, Joe, Jung Suk, Mark M., Mark Z., Nils, Rodolphe, Tristan, and Vincent. Thanks as well to Bartek, John, Marcin, Matthew, Mike, and Sean for the distractions, sweet times, and occasional epiphany. And of course a thank you to my brother and cousins who purportedly taught me everything I know, and to my parents for their unwavering support and encouragement. Funding for this project was provided by Virginia Penhune, Robert Zatorre, and CIRMMT.

Contents

1	Introduction	1
1.1	Electronic musical interface design	2
1.2	Neuropsychology and imaging	3
1.3	Outline	6
2	Background	7
2.1	fMRI	7
2.2	Dangers and technical difficulties	8
2.2.1	Static magnetic field	9
2.2.2	Gradient magnetic field	11
2.2.3	RF electromagnetic radiation	13
2.2.4	Image SNR reduction and artifact generation	14
2.2.5	Ergonomic constraints	19
2.3	Summary	21
3	A survey of MR devices and techniques	23
3.1	Optical sensing	24
3.1.1	Intensity modulation	26

3.1.2	Modulation by polarization	31
3.1.3	Phase modulation	32
3.1.4	Frequency modulation	33
3.1.5	Sensor arrays	35
3.2	Actuators	35
3.2.1	Piezoelectric and ultrasonic	36
3.2.2	Hydrostatic	37
3.2.3	Electrorheologic fluids	37
3.2.4	Electrostrictive	38
3.2.5	Electrostatic	38
3.2.6	Electromagnetic	39
3.2.7	Photostriction	41
3.3	Musical Performance in MRI Scanner	41
3.4	Summary	44
4	Interface design	47
4.1	Design constraints	47
4.1.1	Piano keyboard design parameters	48
4.1.2	Computer mouse design parameters	49
4.2	Design paths	51
4.2.1	Piano keyboard overview	51
4.2.2	Computer mouse overview	64
4.3	Implemented design	66
4.3.1	fMRI-compatible piano keyboard design	66
4.3.2	fMRI-compatible computer mouse design	76

4.3.3	Implemented optical force sensor	77
4.4	Summary	78
5	Device testing, calibration, and recommendations	81
5.1	Testing and calibration	81
5.1.1	General testing	82
5.1.2	Keyboard-specific testing	83
5.1.3	Mouse-specific testing	88
5.2	Recommendations and future work	91
5.2.1	General recommendations	91
5.2.2	Keyboard-specific recommendations	93
5.2.3	Mouse-specific recommendations	95
5.3	Summary	96
6	Conclusions	97
6.1	Summary of fMRI-compatible piano keyboard	98
6.2	Summary of fMRI-compatible computer mouse	99
6.3	Future MR-compatible interfaces	99
6.4	An insight on electronic musical instrument design	101
Appendices		105
A	An introduction to the physics behind functional MRI	105
B	Forces due to magnetic fields exerted on ferromagnetic materials	111

List of Figures

3.1	Optical fibres.	29
3.2	Graded neutral density filter.	31
3.3	Optical strain gauges using interferometry to measure path length-induced phase shift.	34
4.1	Piano keyboard interface.	68
4.2	Reflectors glued to key ends, with keys in varyingly-depressed positions.	69
4.3	Optical cables secured to the keybed.	70
4.4	Sensor subsection block diagram.	71
4.5	Circuit board populated with signal acquisition and processing electronics.	72
4.6	Schematic of analog subsection with power supply.	73
4.7	Key transition state machine.	75
4.8	Mouse interface.	78
5.1	Photodetector output showing repeated notes.	84
5.2	Interface electronics in control room.	86
5.3	Keyboard testing within MR scanner.	87
5.4	Functional MRI scans with keyboard.	88
5.5	Functional MRI scans with mouse.	91

5.6 Interface positioning fixture.	94
A.1 Magnetic resonance in action.	110

List of Tables

2.1	MRI scanner topography.	22
3.1	Optical sensing guide.	45
3.2	MR-compatible actuator guide.	46
4.1	Review of keyboard subsystems.	79
B.1	Demagnetization factors for spherical, needle-like, and flat disk-like ellipsoids.	112

List of Acronyms

ASCII American standard code for information interchange

BOLD Blood-oxygenation-level-dependent

CCD Charge-coupled device

CMOS Complimentary metal-oxide semiconductor

CT Computed tomography

DIP Dual in-line package

EEG Electroencephalography

EMG Electromyography

EMI Electromagnetic interference

ERF Electrorheologic fluid

fMRI functional magnetic resonance imaging

GPIO General purpose input/output

IC Integrated circuit

LED Light-emitting diode

MIDI Musical instrument digital interface

MNI Montreal Neurological Institute

MR Magnetic resonance

MRI Magnetic resonance imaging

OSC OpenSound control

PET Positron emission tomography

ppm Parts per million

PSoC Programmable system-on-chip

RF Radio frequency

RX Receive

SNR Signal-to-noise ratio

TX Transmit

USB Universal serial bus

UART Universal asynchronous receiver/transmitter

Chapter 1

Introduction

Seldom does one get a chance to delve, all at once, into several very different fields of study. Bringing together knowledge from multifarious disciplines in order to achieve a goal or complete a task is becoming more and more common, especially when fusing science, technology, and the arts. Technological advances enable us to express and understand ourselves in new ways. While novel devices are invented, hitherto unknown phenomena are discovered, and new theories are explained, they are exploited by both the artistic and scientific communities, sometimes to great effect. The computer, for instance, has found applications in everything from digital photography and electronic music to genomics and astrophysics. Evolutionary biology has even impacted computational optimization and musical composition through genetic algorithms based on mutations, fitness, and natural selection. Conversely musical improvisation has inspired another class of “harmony search” optimization algorithms [29].

It is no surprise then, that techniques from electrical engineering may be applied to create a musical instrument for use in neuropsychological studies. Whether the end result of the psychologists’ work will impact musical performance pedagogy, therapeutic treatment,

or further elucidate the internal functioning and connections of the brain, it is too early to tell. The presented design techniques and technologies are, however, quite applicable to biomedical interfaces and electronic musical instruments, among others. The goal of the project detailed herein is not to present the psychological findings, but rather to present the first generation of musical interfaces designed for use in brain imaging studies. The scope of this thesis is both broad and detailed: touching upon electronics and optics, functional neuroimaging and nuclear magnetic resonance, and musical performance and instrument construction. While some basic principles are omitted, so are extended details and proofs of complex phenomena, as general and advanced texts are widely available, and references to which have been included where appropriate. This text is directed at an audience familiar with the principles of electromagnetism and electronic devices, though an understanding of piano mechanics and *an* experience playing a piano will certainly facilitate an intuitive understanding of the materials at hand.

1.1 Electronic musical interface design

Musical instruments have long been praised for their ability, in the right hands, to produce sounds of sorrow, passion, and triumph. In the last quarter of the 19th century, experiments in acoustics were already underway which made use of electric instruments [30]. Electric and electronic instruments (the distinction being that the former produces electrical signals derived from acoustic vibrations which are amplified and retransmitted as acoustic signals, whereas the latter synthesize the signals using electronic devices) have come into the mainstream throughout the last century with the introduction of the electric guitar and keyboard-based synthesizers. There is, however, a dearth of electronic instruments outside of those controlled with a clavier-based interface (with the possible exception of

the electronic drum set) that have caught on with any sort of wide appeal. The amazing advantage, as well as the primary hindrance, of electronic instruments is the ability to separate the sound synthesis from the physical human interaction through a mapping layer [42]; the potential being the ability to create any sound with any gesture, the problem is in finding a mapping which allows the performer to build technique and repertoire on par with acoustic instruments.

Though we will not concentrate here on the design of novel instruments, it is useful to first inquire if an electronic emulation of an acoustic instrument can draw near to the feel and playability of its analog. Electronic instruments make use of direct measurement of quantifiable interactions between the interface and the player. These interactions can translate into the onset of notes with pitches, loudness, and timbre controlled by the performer. As well, these measurands which correspond to *how* the performer interacts with the interface, given different feedback schemes, can be studied as behavioural indicators of subject performance and learning.

1.2 Neuropsychology and imaging

Psychologists who study the cognitive processes, pathways, and networks, known as neuropsychologists or cognitive neuroscientists, have turned to music to investigate how the brain handles various auditory, memory, and motor tasks. Musical instruments allow performers to communicate a wealth of information and wonderment to their audience through sound and gesture. The human voice is the first instrument we begin to utilize as we learn to vocalize and later speak. At a young age many children start to play musical instruments such as the violin or piano. We may be amazed at how quickly they take to an instrument, however it is rare for such a toddler to dazzle us on the same level that a professional

musician might. How is it then that musicians learn to play musical instruments, and what is happening inside the brain of a musician as he or she progresses from a beginner, to an amateur, to a professional? This is the bailiwick of cognitive neuroscientists. A prominent technique available to neuroscientists is functional magnetic resonance imaging (fMRI), which provides 3D images of the brain, enabling the correlation of action and thought with localized neural activity. The functional part of fMRI differentiates it from the anatomical magnetic resonance images used clinically in medical diagnosis, and requires many trials to build up a statistically significant response to a specific cognitive task, such as listening to music and tapping along to the beat. Indeed, the brain scans need to be correlated with measurable behaviour changes if one is to link, for instance, motor learning and activation of specific neural centres.

There are other brain imaging and neural activity measurement techniques, such as computed tomography (CT), and positron emission tomography (PET), and electroencephalography (EEG), however the high spatial resolution, intrinsic contrast agent, and lack of potentially hazardous ionizing radiation make fMRI a well-suited candidate to study the neural processing centres and pathways employed when performing music. The drawbacks of fMRI are the poor temporal resolution, limitations on materials that can be safely used inside the scanner environment, and the degeneration of image quality due to subject movement inside the scanner.

An accompanying problem is how to study a musician as they learn to coordinate their motor skills with their visual and aural perception. It seems reasonable enough to observe many pianists individually as they play on a concert grand piano, with many trials over a long period of time to track their learning. But does visual observation suffice? Likely not. Firstly, in order to objectively quantify the musician's progress, the experimenter needs to measure and log the behavioural data of a performance — that is, how accurately is

a subject responding to the stimuli? Or in a more musical sense, is the subject playing the correct notes of a melody with the right timing? If the experimenter is interested in very fine details of the performance, a live human adjudicator will not suffice and is prone to inaccuracy. What of a video and audio recording then? For many studies, this may be sufficient, but it still has its drawbacks. A human adjudicator or even a panel of trained observers may be more accurate when armed with the possibility of judging the same performance with multiple passes, however their ability to quantify millisecond timing differentials is far inferior to a computer's. While audio and visual cues of a recorded performance can be processed and measured with a computer, they may also be obscured by ancillary movements or environmental noise. Digital signal processing may allow the experimenters to tease out seemingly lost data, however this introduces complexities they are likely unwilling to deal with. Regardless, synchronizing the stimuli (be it acoustic or visual) with the recorded audio and video streams presupposes a computer will be employed to merge and process the data.

There are other types of equipment experimenters may introduce to their setup to gain a more detailed description of a musician's performance. Three-dimensional motion capture systems enable the recording of minute changes in position of a subject's digits or limbs of interest and allow the experimenter to track these movements in time with a spatial precision and temporal resolution many times greater than a human observer. Electromyography (EMG) measures muscle contraction and can be used in conjunction with fMRI to measure motor activation during performance or even music imagery tasks [55]. Surface EMG does not provide details of specific muscle fibre recruitment however, it merely provides a measure of correlated muscle activity. A more direct approach to measuring human-interface interaction is by embedding electronic sensors into the interface, enabling data logging for offline analysis, as well as real-time synchronization of stimuli and

feedback.

1.3 Outline

This thesis describes the design and implementation of electronic interfaces that are compatible with a magnetic resonance imaging (MRI) scanner. For reasons explored later, most electronic interfaces do not function properly, and might pose a serious safety hazard, inside the magnetic resonance (MR) environment. The prototype devices were to be used in fMRI experiments which focused on motor learning of musical tasks. These are but the first in a series of iterations towards a more refined set of fMRI-compatible musical interfaces. The two interfaces presented here are a two-button response box in the form of a computer mouse, and an electronic piano keyboard. The mouse was used in a rhythmic tapping task, whereas the keyboard was meant for more general piano performance tasks (e.g. playing scales, melodies, and harmonies). This work, and its parent project, hope to contribute significantly to the fields of music technology, cognitive neuroscience, and biomedical engineering.

This thesis is organized into several chapters: starting with a background in MRI physics and the engineering constraints of the MR environment, followed by a review of fMRI-compatible interfaces. The next chapters deal with design and testing of the interfaces, after which recommendations are made toward improving the prototypes. Finally the concluding section summarizes the project and future work, and is accompanied by some final thoughts.

Chapter 2

Background

2.1 fMRI

Functional magnetic resonance imaging is an application of nuclear magnetic resonance that uses as its contrast agent the endogenous oxygenation levels of hemoglobin. Hemoglobin is the oxygen-carrying molecule contained inside a red blood cell. Neural processes, that is thinking and other metabolic processes in the brain, require oxygen. Oxygen is transferred into the hemoglobin in the lungs and the heart pumps the oxygen-rich blood to the brain. Blood flow is regulated by the rate at which the heart pumps and the dilation of blood vessels. The amount, or volume, of blood in the system is maintained at a fairly constant level unless some trauma causes a sudden loss of blood. However, the amount of oxygen in localized areas of the brain can change measurably during changing mental loads.

It should be noted that fMRI does not measure neural activity directly, the signal obtained during scanning is merely correlated with the proportion of oxygen in the blood in a specific region, which in turn is correlated with the dilatation of capillaries and blood flow in that region. In turn this BOLD (blood-oxygenation-level-dependent) signal has been

found to correlate well with neuronal activation [7, 58, 62]. Shortly after a closely-spaced group of neurons fire together, there is a net increase in oxygenated blood to the region in order to resupply those neurons with the energy they need to fire again the following time. The onset of this hemodynamic response begins about two seconds after stimulus, peaking at about six seconds and falls off at about the twelve second mark [9, 41]. These localized increases in oxygen provide the variation in signal intensity allowing three-dimensional volumes to be imaged over time. For a more in-depth, though basic, explanation of fMRI please refer to Appendix A. Briefly, to elicit an MR signal the volume to be imaged is placed within an intense and uniform magnetic field.¹ Slice selection and contrast protocols are implemented by precisely timing the switching of gradient magnetic fields and exposing the sample to pulsed radio-frequency (RF) energy. MR signal acquisition proceeds by sensing the RF signal emitted from the excited sample volume as it returns to its rest state. The volume is scanned many times throughout an fMRI study in order to measure relative changes in signal levels seen during functional tasks versus a baseline resting state. Statistical analysis is performed after the scans in order to find significant differences between behavioural states and among populations. Attaining a high-quality image requires a strong homogeneous magnetic field, precise timing and synchronization, and a clear RF channel free of noise.

2.2 Dangers and technical difficulties

The design of electromechanical devices is made even more difficult when they must operate within the MR environment. There are three main issues when designing devices

¹This strong permanent magnetic field is also one of the dangers when dealing with MRI scanners and the hazards associated with it and other components of the scanning process will be discussed further in the following sections.

for use in conjunction with an MRI scanner. Firstly, subject and technician safety is the overriding priority in any clinical or experimental setup. Thus the designation “MR-safe” is applied to devices which do no harm to the patient within the scanner. Another issue is any interference of the image that is caused by the device. Due to the highly sensitive measurement equipment and the required magnetic field uniformity, any distortion of the field lines or spurious aberrations thereof will cause a decrease in the signal-to-noise ratio (SNR) or image artifacts. The last issue we will consider is the interference caused by the scanner itself, which might cause the device under test to malfunction or become completely inoperable. Devices that are shown to be MR-safe do not create image artifacts or significantly decrease the SNR, and function uninhibited within the MR environment are given the designation “MR-compatible”. This section will deal with the causes of certain device deficiencies and how to overcome these MR-specific design constraints.

2.2.1 Static magnetic field

The permanent magnetic field in modern MRI scanners is usually generated by a large supercooled superconducting magnet.² Immersed in liquid helium to keep the temperature just above absolute zero, the magnets in the most common modern scanners used in human imaging generate as much as a three Tesla field; around 50000 times that of the earth’s magnetic field. The magnet is a cylindrical shell and concentrates its field inside the bore of the scanner. In functional brain scans, the subject lays on a movable table and the head is positioned at the isocentre of the scanner, where the magnetic field is the most intense and homogeneous. Ferromagnetic materials, due to their large magnetic susceptibility, are easily magnetized and are thus problematic for several reasons within the MR environment.

²It is permanent in the sense that the magnetic field remains, even after the scanner is turned off, contrary to popular belief. Though the magnetic field quickly disappears if the superconductor’s temperature rises above a critical value.

Ferromagnetic materials, such as iron and many steel alloys, undergo forces and torques within a magnetic field, as we are used to feeling with fridge magnets and other surfaces to which we stick them. We may have also noticed that the closer we bring the magnet to the fridge, the stronger the attractive force. Many times more powerful than a fridge magnet, the static magnetic field of an MRI scanner could pull an unsecured refrigerator into the scanner. Though this is not a likely situation, there have been recorded instances of vacuum cleaners brought into the fment by a new member of the night-time cleaning crew or more disastrously oxygen tanks brought into the MR environment in order to resuscitate a patient. In each case, the foreign object containing ferromagnetic material was brought into the scanner environment, through a door that was a significant distance from the bore of the scanner such that the forces acting on the object were initially very weak. However as the object was brought closer to the scanner, the forces increased rapidly³ and the the object was accelerated unstoppably into the middle of the scanner bore, with sometimes fatal results [79]. While the static magnetic field of an MR scanner has not been shown to pose any biological threats on its own (the U.S. Food and Drug Administration has prescribed an eight Tesla maximum field strength on scanners used for human subjects [84]), another potentially fatal oversight may be the admittance of a patient with a ferromagnetic implant or embedded shrapnel. Please refer to Appendix B for a quantification of translational forces and torques on ferromagnetic objects within a magnetic field. In summary, an increase in magnetization proportional to field strength, magnetic susceptibility, and material volume contribute to higher forces. Though ferromagnetic materials positioned in the isocentre of the bore may not undergo translational forces, object geometry and field alignment may be such that the torque produced in concert with the magnetic field will reorient the

³The force (F) versus distance (R) relationship follows a power law: $F \propto R^{-n}$, where n is a constant greater than one.

specimen. This is especially devastating if the object is a human-implanted device. Thus devices brought into the MR environment must be free of ferromagnetic material, unless in extenuating circumstances when the object is sufficiently removed from the scanner bore and properly secured. If at all possible, such materials should be placed outside of the MR environment, in the control room.

There is a curious phenomenon that, while not so dangerous, should be acknowledged here as it may manifest itself in certain mechanical designs. A non-ferrous conductor, such as an aluminium pie plate, placed precariously on its edge inside the bore will try to tip over due to the force of gravity (as it would outside the scanner). If the pie plate is oriented so that its falling motion will cause it to move through magnetic field lines (that is, perpendicular to the magnetic field), the magnetic flux will induce a current inside the conductor. This current (known as an eddy current), in turn, creates its own magnetic field in opposition to the external magnetic field. The net force which acts on the pie plate will still cause it to fall, though at a considerably slower speed. As is the convention in the design of transformers and electric motors, eddy currents can be significantly reduced by segmenting the conductive object into thin electrically insulated slices, or laminations.

2.2.2 Gradient magnetic field

The gradient magnetic field is produced using resistive electromagnets and gives rise to the frequency-encoded spatial information that is germane to MRI. These electromagnets are rapidly switched on and off during scanning and thus give rise to time-varying magnetic fields. As Maxwell's equations imply, any time-varying magnetic field gives rise to a time-varying electric field.⁴ At elevated switching frequencies, peripheral nerve stimulation due to induced currents in tissues, which act as a conductor, may cause subjects to experience

⁴By solving $-\frac{\partial B}{\partial t} = \nabla \times E$ and $\frac{\partial D}{\partial t} = \nabla \times H - J$

anything from a mild tingling sensation to involuntary muscle contractions to cardiac fibrillation. However, the direct health risks and biological effects associated with these fields on the human body are specifically minimized by the scanner itself by way of limiting the maximum switching frequency. The slower fluctuations of the gradient magnetic field reduce the flux and thus reduce the induced current to a level below the threshold needed to stimulate a nerve. The induced current in a stationary conducting loop of N turns within a fluctuating magnetic field B_g is given by:

$$I = \frac{-N}{R} \int_S \frac{\partial B_g}{\partial t} \cdot ds$$

where R is the resistance of the loop, and the flux is integrated over the surface area of the conductor [77].

Again, a current will be induced in a conductive object such as a coil of wire when it is moved within a magnetic field such that it cuts through lines of flux, or if the applied magnetic field itself changes. Furthermore, that induced current will generate its own magnetic field and may be directed with, against, or at some angle to the applied field, causing the object to undergo a translational force and/or rotational torque. A coil of wire with numerous turns induces a greater current due to magnetic flux than a single loop of wire. It is also quite important to take note of the fact that the larger the current in the wire loop (induced by some flux or supplied externally), the greater the magnetic field produced. Such phenomena may be integral or detrimental to the design of a device for use in an MR scanner. It is therefore imperative that designers be fully aware of the consequences of using conductive materials within the MR environment.

2.2.3 RF electromagnetic radiation

The signal output of a radio frequency synthesizer is fed to a power amplifier before it is emitted via the transmitter antenna. As stated before, this high-power electromagnetic signal is tuned to the resonant frequency of hydrogen nuclei, known as the Larmor frequency. Coupling between the RF signal and a conductor (such as a loop of wire) will induce a current in the conductor. At such high frequencies, electrons move back and forth very quickly, bumping into each other as they go. Much (if not all) of this energy is dissipated as heat. If the resistivity of the conductor is not constant along its length, more heat will be produced in the higher resistance portion of the loop. A loop of wire with many turns will induce more current than a single turn, and will have much more heat to dissipate. This increase in heat is also proportional to the oscillatory frequency. Heating also occurs within insulators through dielectric heating. Polar molecules such as water align with the electromagnetic field which alternates and causes the molecules to rotate when excited by RF radiation. The phenomenon, dubbed RF heating, is taken advantage of in microwave ovens and other non-conductive contact-less heating devices.

There have been reports of surface tissue burns caused by RF heating in MRI scanners [53]. The body, which can be thought of as a high-resistance conductor (with the epidermis responsible for the majority of the resistance, as internal tissues such as muscle and organs contain much more water) can be formed into a loop if two points are “connected” via two different paths. For instance, the arms of a subject in the MR scanner would create two different paths from the torso to clasped hands, and thus a conductive loop. As the skin is the more resistive portion of the loop, a patient, so oriented, might receive burns on their palms if that circuit is maintained for a sufficient amount of time while the scanner is in operation.

It is important then that a device designed for use during MRI testing not contain conductive loops which might cause a fire, burn a patient, or destroy itself (or other equipment, for that matter) due to RF heating. As well, devices with affordances that might encourage a subject to hold their hands together should also be avoided. For instance, a piano task which requires overlapping hand positions should be performed with caution, and prolonged hand-to-hand contact should be avoided. Three-hour fMRI scanning sessions are not uncommon and even with direct and understood directions, subjects may become bored, uncomfortable, and forgetful, disregarding basic safety instructions in order to fulfill some habit or behaviour which might even be common everywhere else in life.

Electrical (and/or magnetic) shielding, the process of enveloping a device or conductor in a protective electromagnetic barrier, will reduce the effect of RF-heating (or current induction due to the switched gradient magnetic fields) and allow the use of coils of wire that might be needed for certain types of electromagnetic actuators. Care must still be taken however to ensure any wire leads used to connect a device (or even the leads which connect electromyogram electrodes) be properly shielded, and that even the shields of multiple wires must not cross or come into contact with the subject for fear that the circuit created might cause RF-heating and burns.

2.2.4 Image SNR reduction and artifact generation

The signal-to-noise ratio (SNR) of an MR scanner or a certain scanning protocol is a measure of the noise floor and thus the smallest discernible variation in the actual signal that we wish to measure. Image artifacts are aberrations in the image and can manifest as distortion or warping of an image or as spurious entities (areas of white or black, resulting from signal saturation or no signal at all) within the image itself. The highly-sensitive receiver antenna, in fMRI often a specially-fitted head coil is used, senses the minute

electromagnetic RF signal that is emitted by the hydrogen nuclei in brain tissue as they return to their rest state after being excited. The signal is then amplified, digitized, and stored on a computer where it is processed and a three-dimensional image is generated. The signal is generated and sensed using precisely-timed and near-perfectly formed magnetic fields. Any alteration of the field within the bore of the scanner that might cause the fields to be deformed, reflected, or absorbed will corrupt image data if the perturbation is significantly large (i.e. greater than half the least significant measurable change in signal amplitude).

Nonuniformities in the magnetic field, which cause a reduction (either globally or locally) in the evoked MR emission, will decrease the signal strength and thus the SNR. Other causes of reduced SNR include increases in the noise floor through random variations in the magnetic field or in-band electromagnetic interference radiated by some unshielded electromagnetic device. Error can be generated in the MR signal within the biological specimen itself on a very small scale due to biological processes correlated with the signal of interest (such as certain drugs which might affect blood flow or oxygen content in the brain).

While SNR is mediated by random fluctuations that blur the image, artifacts are caused by abnormalities in the MR signal. Data corrupted by some types of variations can be reconstituted using signal processing, such as small and (relatively) slow variations in head position or small constant spatial deformations in the magnetic field. However the troublesome artifacts are much more insidious, manifesting spuriously in space and time, or by distorting the image so much that the lost data cannot be reconstructed. Devices brought into the MR environment may contain several sources that could cause image artifacts. As before, the farther the device is positioned from the bore of the scanner, the less of an effect it can have on the magnetic field and thus the potential to create significant artifacts is

reduced.

The most significant contributions to image artifacts from devices brought into the scanner environment are ferromagnetic materials, conductors, and environmental RF noise. Conductive materials, because they induce a current when in the presence of a time-varying magnetic field (i.e. the gradient field) and thus generate their own magnetic field, may cause image artifacts. This is the same for conductors that are conveying signals into and out of the MR environment, as a current carried by a conductor creates its own magnetic field. The MR imaging process requires that the gradient magnetic field establishes a linear relationship between position and the Larmor resonance frequency. When a local magnetic field is generated, especially for a brief instance while scanning, the linear relationship between position and resonance frequency may no longer hold and so the image generated will not represent the actual specimen being imaged.

While diamagnetic and paramagnetic materials are able to bend the magnetic field lines, causing inhomogeneities in the static magnetic field, the gradient field, and the RF field, these effects are small compared to deformation of the field lines due to ferromagnetic materials. Inhomogeneous fields not only produce spatially-aberrant artifacts, but contrast intensity artifacts as well. Because the signal strength of the T2* signal used in fMRI is dependent on the magnetic field homogeneity, if the magnetic field is more homogeneous in one part of the bore than in another, those two portions of the image will have different amounts of contrast, with the less homogeneous portion of the image being darker than the rest of the image.

Yet another issue with respect to magnetically permeable and conductive objects within the scanner is that they can act as shields to the magnetic fields or the RF radiation. If such objects are within the volume that is to be imaged, then they may appear as white or black shapes and any data collected from those voxels would be useless.

We have mainly been discussing non-moving objects, as on their own they can wreak havoc on the MR image. However these problems are only exacerbated when these deleterious foreign bodies are in motion during a scan. While scanning a complete volume may take several seconds, movement during that time may create image artifacts. Movement artifacts arise from patient respiration, blood flow within the body, and any gross movements of the body. In addition, the movement of magnetically susceptible materials or those which might absorb or reflect RF energy could create image artifacts if they are moved sufficiently quickly near the volume being imaged. For this reason it is important that during tasks requiring subjects to move their fingers, for instance, they do not move their whole arm and thus their head. Interface affordances or experimental tasks should therefore ensure the subject remains as still as possible, with extreme stringency shown when motion of the volume to be imaged is involved.

RF noise sources including motors and wired or wireless transceivers are also possible sources of image artifacts. Not only will a constantly turning motor within the MR environment decrease SNR, it may generate periodic or quasi-periodic emissions that could interfere with the precisely timed MR signal acquisition. While it is sometimes necessary to incorporate electrical communications systems into the device design, proper shielding, filtering, and the use of appropriate channels (i.e. frequency bands and propagation modes) are necessary to ensure electromagnetic interference is minimized.

Device operability within actively scanning MR environment

Assuming we have ensured that the device presents no danger to the subject, technician, and equipment, and assuming we have minimized any image artifacts and SNR degradation, are we certain the device itself will work properly within the scanner environment? Device testing outside of the scanner environment is insufficient for determining how it might

function within the scanner. Even testing a device in one scanner environment, specifically testing the device in a lower-field than that in which one intends to use the device, is insufficient in determining how it might function within another scanner environment. While an interface might function properly outside the scanner, or within a $1.5T$ scanner, it may be adversely affected by the fields in a $3T$ scanner and cease to function.

Using magnetically-sensitive equipment, such as magnetic media or hall-effect sensors, in the MR environment may cause total malfunction of the interface due to the extremely intense magnetic fields. In the event that the static fields do not cause device malfunction, the switched gradient fields might very well induce deleterious effects upon such magnetically-sensitive equipment. Electronic components, such as sensors, actuators, or transmission equipment may also be adversely affected by the switching gradient fields, either due to induced noise (so much as to cause erroneous measurements) or catastrophic failure due to device heating by induced current. Device heating due to induction of the RF emissions are another source of catastrophic failure, especially where loops of wire are involved.

The most likely cause of device malfunction, however, is electromagnetic interference (EMI) at radio frequencies. The RF emission bandwidth and signal intensity are significant design obstacles for electronic devices. Electronic communication (or sensing) may fail due to a decreased SNR or due to sporadically induced current spikes causing symbol misidentification. Again, proper shielding, balanced or differential transmission, and relegating electronic components to the control room are possible solutions for such problems, and *in situ* testing is a must.

2.2.5 Ergonomic constraints

MR safety and MR compatibility are paramount in the design of devices intended for use in the MR environment, however there are several additional constraints beyond those discussed above that may be overlooked during the early stages which could prove critical later on. Undergoing an MRI scan can be quite a traumatic experience for people who do not deal well with small enclosed spaces, where they must remain as still as possible for up to three hours at a time, while being bombarded with the loud grating sounds resulting from the scanning process itself. While psychological MR studies are usually performed on healthy subjects, there may arise times of anxiety, medical emergency, or equipment malfunction (such as a cryogen purge) whereupon the subject must be quickly extricated from the scanner. In such cases it is important for an interface, placed over the subject and fixed to the bed of the scanner table (in order for it not to shift and thus create movement artifacts during scanning), be removed easily and quickly so as to allow access to the patient and expedite their extraction.

As was mentioned previously, one must be careful designing experiments that require the subject to move part of their body, their hands for instance, as the subject may be more likely to move their whole body or clasp their hands. Motion transferred from the movement of hands to the shoulders and head could lead to significant motion artifacts. Either restraining the arms at the elbows or designing an interface wherein the palms may rest apart while allowing fingers the reaching and lateral motion they require for the task are possible solutions (such as typing at a keyboard). Tasks which would ordinarily require large movements are not feasible, firstly because there is just not enough room in the scanner bore for the subject to move, and secondly such movements would create motion artifacts in the image, thereby degrading experimental results. “Sparse” temporal

sampling is a technique that has been developed to combat motion artifacts and auditory interference from the scanner by taking images appropriately spaced in time [36].

Subject comfort may have a large impact on the behavioural results obtained from studies, especially if one is measuring performance of a task that the subject is used to completing outside of the scanner. Conventionally, in most MRI scanners, the subject is lying supine in a small enclosed space with limited range of motion. As the subject's orientation has changed from the usual performance posture, so too have the relative directions of gravitational forces on limbs and digits. This may impact subject performance and fatigue. For instance, to keep the hands at the right position and the wrists at the correct angle for piano performance, the arms will have to work harder while lying supine as the shoulders and back muscles are not able to provide the same postural relief. The limited range of motion available within the scanner will constrain the subject and in turn the subject may change their usual pattern of movement to complete a motor task. Lastly, the subject will likely incur increased stress levels as they are confined to a small space, asked not to move, and subject to increased noise levels. While the subject may respond well during the task, fMRI experiments usually require rest periods during which scanning is also performed to contrast rest states with active states. During the rest periods, this type of environment may cause the subject's mind to wander and ignore instructions not to clasp their hands or fidget with the interface. It is therefore important to design a robust interface that cannot be tampered with, and one that does not encourage fidgeting or other unwanted or dangerous behaviour.

2.3 Summary

In this chapter we introduced functional magnetic resonance imaging, a technique which aims to correlate cerebral blood flow with neural activity in order to map parts of the brain to cognitive tasks. Magnetic resonance imaging is a technique that exploits differences of magnetic susceptibility in human tissue to produce image contrast.

An MRI scanner has three main components in addition to the computerized control system: the static magnetic field, the switched gradient magnetic field, and the RF antennas. Each component presents its own difficulties toward designing an MR-compatible device, in terms of safety, image quality, and device functioning. These factors are summarized in Table 2.1.

Ergonomic constraints were also discussed, pertaining to subject comfort within the confined space of the scanner bore and minimizing subject movement during scanning. Safety concerns due to overlapping limbs, and device robustness in the face of idle hands were also discussed.

In the next chapter we will look at various sensing techniques suitable for MRI-compatible devices, as well as review many of the interfaces that have been implemented as part of this burgeoning research field.

Scanner Component	Static magnetic field	Gradient field	RF antennas
Description	Very-high field strength is basis for MR signal	Slice selection and spatial image encoding	RF energy excites tissue; detects MR signal
Potential danger	Strong forces and torques on ferromagnetic materials	Induces current, peripheral nerve stimulation	RF heating, may lead to burns
Image degradation	Decreased field homogeneity distorts image, decreases SNR	Spurious magnetic fields distort image and create artifacts	Magnetically permeable objects create artifacts; EMI reduces SNR
Device malfunction	Position and orientation-dependent response to static magnetic field	Time and spatially-dependent response to magnetic field; current spikes induced in circuitry	EMI causes symbol misidentification, reduces SNR; RF heating, fire

Table 2.1 MRI scanner topography.

Chapter 3

A survey of MR devices and techniques

For little more than a decade now, researchers have been trying to implement MR-compatible devices for surgical tasks, patient rehabilitation, and brain mapping studies. While many tools, like biopsy needles for instance, undergo relatively minor design changes in order to be classified as MR-safe (the change in material of a biopsy needle from a ferromagnetic stainless steel to a non-ferromagnetic alloy), the design of other devices must be completely rethought. An early fMRI study into the neural correlates of a motor task conducted by Ludman et al. [56] used an extrinsic resistive force to oppose finger flexion. This study required the construction of an interface that allowed the subject to grip and squeeze a plastic handle with the fingers (opposing the thumb about a fixed wooden post) while weight of a variable mass was presented to counter the finger flexion over a distance of a few centimetres. Interestingly, the study used a system of pulleys (and presumably nonconducting cables) to connect the handle inside the scanner to the weights outside of the scanner environment where the experimenter was able to change the applied weight. The study also

mentions that the flexion-extension task was repeated at 1.3 and 1.7Hz , however there is no information given as to how the accuracy of the repetition rate was measured. This type of task is common in the literature, and we will see how the interfaces have evolved to sense not only one-dimensional flexion forces, but also torques and higher dimensional forces in addition to applying electronically controlled counter-forces, toward MR-compatible haptic devices.

3.1 Optical sensing

Sensing within the MR environment has long included optical sensing [24, 73, 74]. In its most basic form, optical sensing enables the remote transduction of forces or motion by modulating light intensity that is both transmitted and received via optical fibres. However, more advanced optical sensing techniques exist which make use of polarization angle, interferometry, and spectral or timing information. Due to the relative wavelengths of RF and optical electromagnetic radiation, and the effective bandwidth of optical measurement systems and transmission lines, optical systems are virtually immune to effects of the MR environment. An exception would be magnetostrictive fibre optic cables that would affect the fibres' properties and thus the transmitted signals within a magnetic field. As well, due to the effective bandwidth of the MR measurement system, the optical signals have no effect on image SNR and field homogeneity.

Fibre optic cables allow optical signals to be transmitted for long distances while maintaining signal integrity. Thus signals are sensed in the MR environment by running cables between the MR scanner and the control room: one sending light into the scanner environment whereupon it undergoes some modulation and is then transmitted back down another cable. The received signals are transduced optoelectronically using standard (and usually

not MR-compatible) electronics outside of the MR environment in the control room. Chappuis et al. have shown that sensing of forces and torques, even in multiple axes, are possible in many different configurations and for many different applications using optical sensing techniques [11].

Optical sensing is unmatched by other techniques when considering sensitivity, bandwidth, and diversity of applications. Optical technologies enable contact, non-contact, and remote sensing capabilities; a feature not shared by piezoelectric, resistive, and capacitive sensors. As noted previously, optical sensing generally operates on the basis of an emitter or light source which launches photons toward some optical modulation mechanism and the modified optical signal that is measured by a receiver. While optical devices exist to measure acceleration and force, even microfabricated packages often do so through measurements of position. Optical force sensors commonly make use of strain gauges which have characterized deformation parameters whereby the variation of the variation in light transmitted through the system is proportional to the extent of the deformation, indirectly measuring the loaded force. Some accelerometers function in a similar fashion by measuring the displacement of a reference mass due to its inertia while in motion. The variation in light transmitted through the system is often compared with a known optical reference path in order to decrease sensitivity to unwanted disturbances (e.g. temperature). Sensors can be arranged in a differential manner, such that their outputs vary in opposite polarities, in order to increase SNR and common-mode rejection. The change in received light with respect to transmitted light, modified by what we have referred to previously as the modulation mechanism, can manifest as changes in intensity, polarization, phase, and frequency. The quantum mechanical basis upon which optoelectronic semiconductor physics is based, and an explanation of the creation and transduction of light by the emitters and receivers is beyond the scope of this discussion. Should the reader wish, a number of resources are

available on the subject [22, 68]. In this section, common sensing techniques are presented, with a special focus on fibre optic sensing, however this detailing should not be taken as an exhaustive list [35, 83].

3.1.1 Intensity modulation

Intensity measurements (i.e. those that quantify the number of photons collected by the receiver) can be performed using a variety of devices including photovoltaic cells, resistive photocells, photodiodes, and phototransistors, as well as photo-multiplier tubes. These devices convert the amount of light into a proportional electrical signal. When measuring ambient light or when using a source with a wide spectral bandwidth, care should be given to the frequency versus intensity sensitivity curves stated in the device datasheet, as well as the intensity-to-output signal curves, as they often represent non-linear relationships. For this reason it is advantageous to employ an emitter with a narrow bandwidth: a light-emitting diode (LED) over a white-light source, or better yet, a laser. Measured intensity can be varied in a number of different ways, for instance: distance between emitter and receiver due to dispersion; angle between emitter and receiver which varies the number of absorbed photons incident upon the receiver; transmission losses due to changes of index of refraction of the propagation medium; transmission losses due to occlusion which cause photons to be absorbed, scattered, or reflected.

Even collimated beams of light — those arising from a point source whereby they all travel in the same parallel direction — in practice, have a focal point, and thus either converge or diverge at some relatively large distance. Thus the irradiance of a collimated beam decreases, however gradually, as a function of distance. For example, a laser beam that begins to diverge promptly upon exit from a collimating lens arrangement will have a larger spot size at $100m$ than it does at $50m$. Given that the wavefront at $50m$ contains the

same optical power that it does at $100m$ (assuming no transmission losses), the intensity of light, absorbed by a detector of nominal surface area less than the spot size placed normal to the beam, will be greater at $50m$ than at $100m$.

The angle between the surface of the receiver and the incident beam of light affects the amount of light absorbed by the reflector due reflection and refraction. If the surface of the receiver is flat and the distance between the top of the passivation layer and the optoelectronically-active layer is significant, then the only angle at which all of the light is transferred into the optoelectronically-active cavity is perpendicular to the planar surface. At any other angle, a portion of the light is reflected back from the surface, and the light that enters the optical cavity will be refracted at some angle dependent on the ratio of refractive indices. Depending on the geometry of the optical cavity, the refracted light may veer away from the optoelectronically-active surface. In applications where angle-dependent intensity modulation is unwanted, these issues are often dealt with using lenses that collect light coming from different angles and focus the beam onto a point within the sensor.

Consider a fibre optic cable which connects the emitter and receiver. The fibre optic cable is composed of two parts: the core having a higher index of refraction than the surrounding cladding. The fibre is often coated in a protective layer or jacket to increase the strength and ruggedness of the fibre, though they do not affect the optical path. Fibres are commonly made with glass, quartz, and more resiliently with plastic. Light is launched into the core by the emitter and through total internal reflection is kept within the fibre with very little loss over long distances, as shown in Figure 3.1 (A). Losses are increased significantly by bending the fibre so that the beam's angle of incidence is smaller than the critical angle for total internal reflection, thus a portion of the light is lost to the cladding (compare the untreated sections of Figure 3.1 (B) and (C)). This phenomenon

can be exploited to create an optical bend sensor whereby modulation of light sensed at the receiver is dependent on fibre flexion. While bending losses are small for obtuse angles, sensitivity can be increased by treating a portion of the fibre (i.e. the section that is to be bent) by removing the original cladding (through notching, abrasion, etching, etc.) and replacing it with a material having a higher index of refraction. This leads to an irregularly formed surface through which light can escape and an increased critical angle, such that the effect of total internal reflection is reduced at the bend point where the incident angles are smaller (compare the treated sections of Figure 3.1 (B) and (C)). The “Shape Tape” and “Shape Hand” and other fibre bend sensors made by Measurand Inc. make use of arrays of such sensors. The technology, originally developed at the Canadian Space Agency, uses loops of treated optical fibres, each acting as a bend/twist sensor with light being emitted into the channel at one end and the light intensity measured at the other [21]. As the device is bent about a specific point, the optical fibres sensitive to bends in the specific region give up a certain amount of light to the cladding due to the treatment of the fibre. The treatment may consist of several closely-spaced notches to decrease the unbent losses, and increase loss linearity with increased curvatures. The loss of light is proportional to the bend angle at the treated location, and since different fibres are treated at different points (and orientations) along the length of the device, the bends, twists, and overall shape of the interface can be decomposed mathematically, and a three-dimensional representation can be constructed. Other optical force sensors rely on microbending losses in untreated fibres [6].

Obstructing light emanating from the emitter with respect to the receiver blocks some or all of the light that would otherwise be absorbed by the sensor. There are several ways to accomplish this feat through reflection, refraction, and absorption. The simplest means to decrease the amount of light incident upon the receiver is to place an opaque or reflective

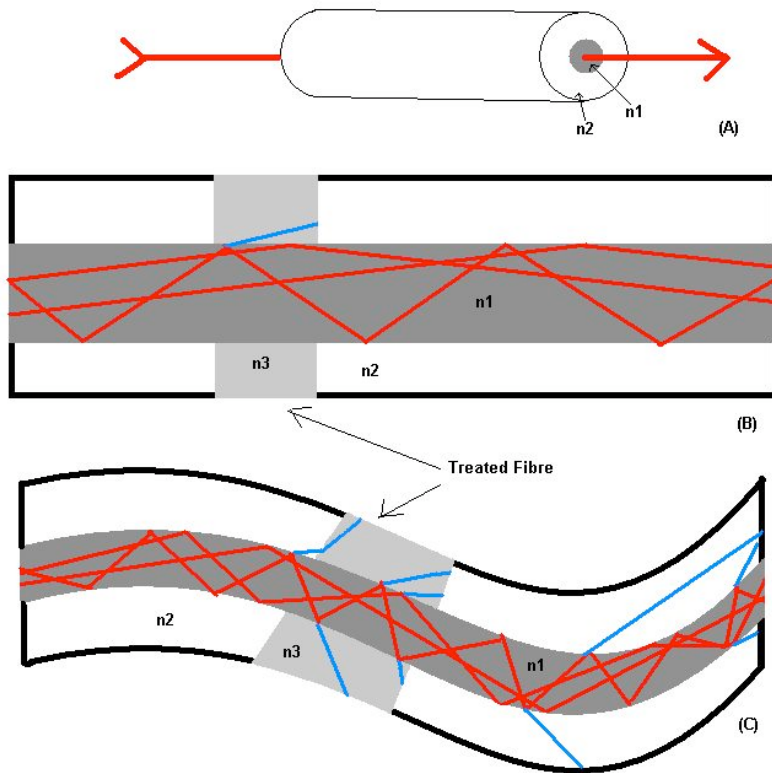


Fig. 3.1 Optical fibres.

(A) straight untreated fibre conveys nearly all input light to output; (B) unbent fibre has losses at treated interface with low angle of incidence with respect to the normal, little loss elsewhere; (C) bent fibre has losses at bends due to decreased angles of incidence and more so at treated interface due to increased critical angle. Refractive indices: $n_1 > n_3 > n_2$

blind in front of the receiver so that when in place all of the incoming light is reflected or absorbed by the blind and when removed, the light is transmitted to the receiver. Similarly, if the emitter and receiver are both facing the same direction, as opposed to each other, light intensity can be increased by placing a mirror which reflects the outgoing beam of the emitter back to the receiver, and when removed, no light is incident upon the receiver. Interfaces made by Tactex Controls Inc. make use of a porous foam into which light is shone via an optical fibre and collected with another [45]. The foam membrane, which

makes up the deformable surface, may be depressed, whereupon light is scattered with increasing intensity. The back-scattered light, conveyed by the efferent optical fibre, is detected using an optoelectronic device and converted into an electronic signal. Several pairs of optical fibres are organized about a single membrane to increase force sensitivity and aid localization.

An optical quadrature encoder is a device that transduces translational or rotational movement as a sequences of binary pulses, from which position and velocity can be deduced. An optical encoder uses a series of alternating transparent and opaque (or reflective and non-reflective) segments printed on a linear or circular track through which light is periodically sensed as the track is moved transversely between the emitter and receiver. Using multiple tracks and receivers, absolute position can be obtained, or with a single track and two receivers, incremental position can be measured. Optical encoders are often used instead of potentiometers where the friction caused by the wiper would quickly wear out the resistive material prematurely, and thus the contact-less optical encoder would provide a much longer lifetime (e.g. guitar volume/wah pedal).

A graded or graduated neutral density filter is an optical filter that passes a large flat spectrum with spatially-varying degrees of attenuation. The gradient can be stepped or smooth along its length (for a rectangular shape). A laser beam launched toward a photodetector placed behind a graduated filter would be only partially transmitted to the detector, the attenuation dependent on the filter's placement, thus absolute position (and from there velocity) may be measured. A similar setup is shown in Figure 3.2, though it shows four lasers and detectors for visualization purposes, a single laser and detector would suffice to measure position with an absolute error of one-half the width of a gradation.

Replacing the filter in the previous setup with a system of lenses and/or prisms to focus and direct the laser beam, the detected light intensity may be modulated by the positioning

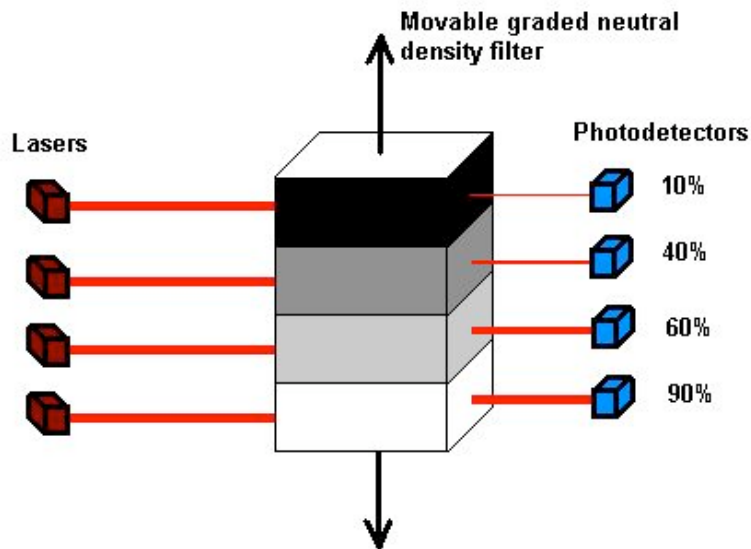


Fig. 3.2 Graded neutral density filter.

A setup consisting of four lasers aligned with respective photodetectors, bisected by a movable graded neutral density filter. The four filter gradations transmit 10%, 40%, 60%, and 90% of the incident light, respectively. By shifting the filter up or down, a change in intensity at a given photodetector may be achieved.

and orientation of the optical system. This type of system modifies the amount of light collected by the receiver either by deflecting the beam onto or away from the detector, or by diffusing the beam so that it is less intense at the detector.

3.1.2 Modulation by polarization

Polarization angle and type can be modulated using specialized optics and electromagnetic fields, however sensing of such changes is commonly performed with intensity measurements after passing the light through a polarizer of known angle. Without delving too deeply into the physics of light propagation, we consider that a traveling light wave has two transverse components that propagate longitudinally at the same frequency. These two

components may have different relative phases and amplitudes, which determine the wave's polarization. An incoherent beam of light is made up of many such light waves, each with uncorrelated polarization relative to one another. If we pass an incoherent beam through a polarizer (or polarizing filter), we effectively decrease the amplitude of one of these transverse components to zero and completely pass the orthogonal component unchanged (intermediate polarization angles are gradually attenuated). If we then place a second polarizer after the first, and rotate the former with respect to the latter, we modulate the light intensity passed through the second polarizer by an amount dependent on the angle between the filters' polarization axes. Light can be totally occluded if one polarizer is rotated at a right angle to the other, or can be passed if they are aligned. Angles between zero and 90 degrees will produce some intermediate attenuation. Although polarization-maintaining optical fibres exist, they are expensive when compared to ordinary fibre optic cables. Additionally, for use in an MR environment, one must be aware of the Faraday effect: the rotation of the polarization plane within a magnetic field. This phenomenon does however allow optical measurements of temperature and magnetic field, which may be of use in MR-compatible interfaces.

3.1.3 Phase modulation

Interferometry is a technique used to measure phase changes of light through some medium. Consider a beam of light that is split into two paths. One undergoes a change in phase with respect to the other, and following that they are recombined. When the two beams are superimposed, an interference pattern is created with successive peaks and nulls corresponding to constructive and destructive interference. In practice, interferometry is performed with a narrow band of coherent frequencies, such as the light from a laser split into two beams, so that instead of appearing as spatial interference bands, the interference

corresponds to a change of intensity. Broad-spectrum interferometric techniques, however, are also common. Phase changes can be effected by lengthening or shortening the optical path under test with respect to a constant reference path, or placing an object of certain optical properties within the test path. The change in intensity due to interference is of course related to the change in phase and the nominal wavelength of light launched into the system, and consequently is periodic in nature. This periodic ambiguity can be overcome using low-coherence interferometry.

An example application for MR force sensing consists of a test path with a compressible optical medium. As the medium is compressed by an applied force, its optical path length is shortened, thus inducing a phase change. When the phase-shifted beam is combined with that from the reference path, the light intensity due to interference is proportional to the relative phase shift. Figure 3.3 shows interferometric techniques, using laboratory equipment (top) and optical fibres (bottom), to implement an optical strain gauge. By selecting an appropriate wavelength of light, material properties, and geometry for a range of applied forces, the compressible medium can be matched to provide an optimal dynamic range without periodic interference patterns. A fibre-optic microphone was developed based on a Fabrey-Perot interferometer and low-coherence infrared emitting diode for aircraft noise spectra discrimination [25].

3.1.4 Frequency modulation

A fibre Bragg grating can be used to measure force and temperature, we will consider only the former case here. A fibre Bragg grating is an optical filter which reflects a narrow band of frequencies. By applying a longitudinal force, causing the sensor to strain, the filter's centre frequency is altered. The periodic modulation of the refractive index, built into the core of the fibre, along with the length of the grating determines the centre frequency, and

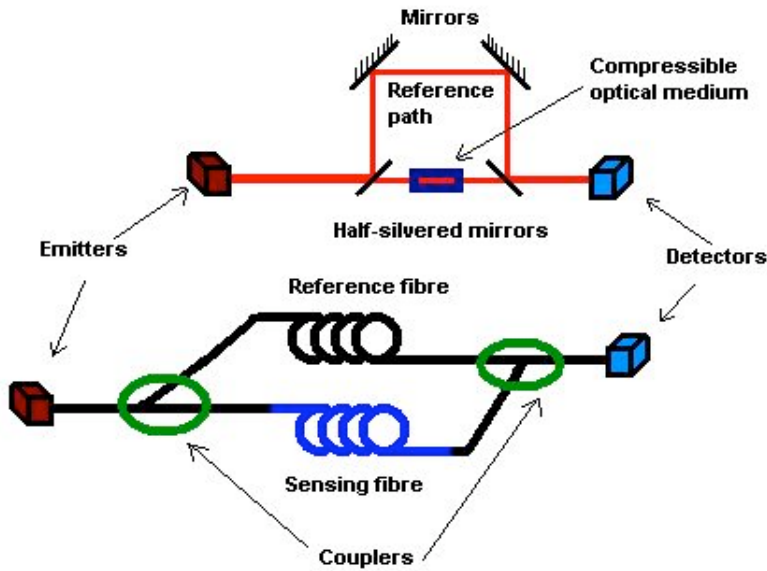


Fig. 3.3 Optical strain gauges using interferometry to measure path-length-induced phase shift.

A coherent light source is split into two paths: a reference path and a sensing path. The length of the sensing path decreases with an externally-applied force, causing a change in relative phase between the two beams which are combined at the detector. Constructive and destructive interference, dependent on the phase shift, results in modulation of beam intensity at the detector. The top diagram employs laboratory equipment and an optical medium that provides a compression-dependent phase shift, while in the bottom diagram the strain gauge is embedded within the optical fibre.

when the grating is compressed or elongated, the grating length and period are modified. The fibre can be interrogated by sweeping the frequency of the input beam (usually a tuned laser) and measuring the intensity at each wavelength that is reflected [19], though this is a slow process easily corrupted by fluctuations of optical input power and non-uniform photodetector sensitivity. More robust interrogation schemes make use of wave-division multiplexing, reflectometry, and interferometry [1, 49, 61].

3.1.5 Sensor arrays

The most common optical sensor arrays are CCD (charge-coupled device) and CMOS (complimentary metal-oxide semiconductor) cameras. These devices are made up of a two-dimensional grid of light sensors. A linear CCD sensor is a one-dimensional array of optical sensors. Using proper lensing and coherent fibres, an image can be piped from its origin to a camera in a location removed from a hazardous environment. A very simple setup to detect position and movement might include using computer software to recognize bright spots or cast shadows detected by the camera. Using high-speed acquisition techniques and an array of photodiodes, sensing the vibration of musical instrument strings is possible [37].

3.2 Actuators

Actuators — transducers that convert potential energy (usually electrical) into kinetic energy — are essential for haptic and robot-assisted surgery systems. Actuators may run “open-loop” where they are directed by a control signal in a preconceived way, or they may be operated in a “closed-loop” system whereby decisions about the actuator’s control are determined through feedback from a sensing system. For safety reasons actuators are often run using at least some sort of limiting, such as temperature, current, or extension limiting for a linear actuator which has exceeded its normal operating range and might destroy itself otherwise. The control system may be simple or complex, but its effectiveness is also partially determined by the sensor and actuator characteristics. Here we present several MR-compatible actuation techniques.

3.2.1 Piezoelectric and ultrasonic

The development of robot-assisted MR procedures has seen the introduction of various technologies to the MR environment. An early version of a surgical-assist robot created by Chinzei et. al [17] used non-ferromagnetic metal alloys, plastics, and piezoelectric ultrasonic motors, to create a five degrees of freedom catheter positioning system. Movement in each direction was sensed optically and transmitted via optical fibres out of the scanning environment to optoelectronic circuitry. The motors which directly actuated the linkages were positioned one to two metres from the imaging volume in order to reduce the possibility of image artifacts created by the motors and currents. The ball screws and linear motion guides transmitted forces to autoclavable rigid arms that attached to the surgical implement. Testing revealed that the moving robot reduced field homogeneity by 0.08ppm (parts-per-million), from a baseline inhomogeneity of 0.45ppm to 0.53ppm , whereas the field homogeneity with a human participant inside the scanner was measured at 1.4ppm . The robot decreased the SNR by 1.6% to 1.8% [16].

Pfleiderer et al. created a robotic system for biopsy and interventional therapy of mammary lesions [66]. The device used piezoelectric motors to position a needle affixed to the actuator in two spatial dimensions. The device produced no significant artifacts and its operation was not adversely affected by the MR environment. However, the MRI-guided system was not designed for real-time closed-loop control. Conversely, subjects were placed in the scanner, and suspect lesions were detected and localized by a radiologist. The coordinates of the lesions were input to the control system to robotically position the biopsy needle and the biopsy was performed manually. This two-stage procedure is sensitive to tissue shifting between imaging and needle positioning leading to suboptimal results.

3.2.2 Hydrostatic

Hydrostatic actuators have also been applied to MR-compatible interfaces, as the power source can be located outside of the MR environment and transmit large forces to the end effector within the scanner. However the drawbacks to this method include the nonlinear control dynamics and sluggish response because of its low-pass characteristics [26, 27]. Burdet et al. continued this hydrostatic exploration by designing hybrid haptic interfaces utilizing hydrostatic force transmission with ultrasonic motors [10]. Their design employs fibre optic force, torque, and displacement sensing. Force and torque were measured by modulation of reflected light, while displacement sensing was accomplished with a rotary quadrature encoder.

3.2.3 Electrorheologic fluids

Electrorheologic fluids (ERF) are viscous suspensions whose viscosity can be modulated under an externally-applied electric field. They have been used in MR-compatible devices to provide variable resistance in hand grip-force experiments [50]. The device employed an optical rotary encoder to measure angles, velocities, and acceleration of the hand. An aluminium strain gauge was incorporated into the device to measure isometric forces. ERF technology introduced shielded high-voltage lines into the MR environment (up to $5kV$ in their testing) however due to the low currents (below $150\mu A$) and because the interface was situated at arms length from the imaging volume, artifacts, and SNR reduction were negligible. It should be noted however that SNR testing was done with a phantom¹ and not using functional data. fMRI scans are more sensitive to reductions in SNR and field

¹An MRI phantom is a specially fabricated volume containing water or paramagnetic gel that produces an MR signal when scanned. They are used as a nominal reference volume, with known magnetic properties, to characterize the scanner.

homogeneity than anatomical scans as Gassert et al. point out [27]. An MR-compatible hybrid haptic device incorporating ERF, an ultrasonic motor, and an optical position encoder was demonstrated [12]. This device allowed fMRI investigation of human motor control and circumvented some of the problems associated with the hydrostatic force transmission mentioned above (namely friction and compressibility owing to decreased bandwidth). The device bandwidth was quoted as several hundred Hertz, however MR-compatibility data was severely lacking. In order to design an MR-compatible haptic interface with sufficient bandwidth to compete with commercially-available devices (i.e. those that are not MR-compatible), the device must have a corner frequency of at least 500Hz in order to make use of the 1000Hz control rate [14]. Current work by Gassert's team is the development of such a device, however their most recent installment as of this writing is not yet in the MR-compatible stage, however it does promise the requisite bandwidth [13].

3.2.4 Electrostrictive

Electrostrictive materials are able to deform under an externally-applied electric field. An MR-compatible actuator utilizing an electrostrictive polymer was designed and incorporated into an MRI head coil to allow reconfigurable coil placement about the subject's head for optimized image quality [80]. Several single actuators may be stacked and controlled in a binary fashion allowing for many easily-controlled stepped deformations over a large range. While this setup obviates limit sensing, feedback, and complex control systems, it introduces high-voltage potentials into the MR environment.

3.2.5 Electrostatic

Electrostatic actuators function by applying a large potential difference across two parallel plates, thus creating an electric field which gives rise to an electrostatic force. By patterning

an insulating substrate with triples of interdigitated copper traces, a three-phase linear motor was designed and tested within an MRI scanner [82]. The device operated without significant reduction in image SNR within a $1.5T$ scanner when the device was operating below $1kV$ at $35cm$ from the RF-coil. However, at higher driving voltages and when placed closer to the isocentre of the magnet bore, the device caused significant decreases in SNR. Interestingly, though the authors state that their device is successful, they mention in passing that a driving voltage above $1kV$ is necessary to obtain forces with a sufficient magnitude to be practical.

3.2.6 Electromagnetic

Lastly we will discuss electromagnetic actuators which make use of the scanner's large static magnetic field to produce Lorentz forces within current-carrying conductors. While electrostatic actuators and other technologies that operate using large electric fields require high voltages, the force generated within an electromagnetic actuator depends on the current and external magnetic field. Within the MR environment specifically, high currents are not required because the magnitude of the magnetic field is so large. A hand grip haptic MR-compatible interface was developed by Reiner et al. [67] that used electrified coils of wire to generate torques of up to $4Nm$. The control system used an optical rotary encoder as well as an optical force sensor. Force sensing was accomplished by measuring the ratio of light received between two adjacent and parallel optical fibres, while the transmitting fibre, which faced the receiving pair, was moved along the parallel plane. With currents below $1A$, and the device placed $1m$ from the isocentre of a $3T$ scanner, reductions in SNR were insignificant, however there is no mention of deterioration in field homogeneity. As well, SNR testing was conducted with a constant current, and not with the varying currents that would be characteristic of normal operation during haptic tasks for which their complicated

control systems were designed. It is also important to note that due to the vector nature of the static magnetic field, different orientations of the device (and time-varying effects due to varying gradient field strength) will generate disparate actuator forces.

Electromagnetic actuators are not impaired by the same internal compliant and frictional energy losses associated with some of the above technologies, and as such, their operational bandwidth can be much higher. Electromagnetic actuators can therefore be used to generate vibrotactile stimulus in somatosensory MR studies. An electromagnetic vibrotactile actuator detailed in a paper by Graham et al. [34], it is explained, has several benefits over other somatosensory stimulators. They note that piezoelectric vibrators provide insufficiently small displacements for their type of study; compressed air and manual stimulation do not yield repeatable tactile results. Their device, which consisted of a pair of coils, was tested in a $1.5T$ scanner and showed no decrease in SNR when the actuator was strongly-driven. Though they provide the driving voltages used in the experiment ($50mV$ to $250mV$) and qualify that the vibration intensity increases with increased input voltage, unfortunately, they do not quantify those forces nor the associated driving currents (nor do they list the coil impedances or field intensity/distance from the isocentre). Encouragingly, the wires that power the actuator are shielded, and a filter (with a stop band of $17kHz$ - $100MHz$) is incorporated to ensure gradient field switching and RF pulses do not cause erroneous actuation. As well, it is noted that the positioning and orientation of the actuator determines the applied force vector, and a solution to this limitation is proposed which would implement three orthogonal coils enabling forces to be generated in arbitrary directions. The system would be calibrated by driving one coil and sensing the induced current in the other two coils. This actuator was adapted for an fMRI study involving a virtual reality environment consisting of the actuator mounted on an optically-sensed data glove, and a pair of fMRI-compatible goggles projecting a stereoscopic image [52].

The optical sensing of finger flexion was accomplished using “Shape Tape” developed by Measurand Inc, as described previously.

3.2.7 Photostriction

One final note on a technology seemingly not yet explored in MR-compatible actuation, that of non-ferromagnetic photostrictive materials. Photostrictive or opto-piezoelectric bimorphs deform when excited by high-energy photons (i.e. ultraviolet frequencies and above). The photons are absorbed by the top layer of the irradiated surface and a current is induced due to the photovoltaic effect. The induced current generates an electric field across the two layers causing the bimorph to deform due to the converse piezoelectric effect [76]. Though the frequency response of such an actuator would be limited (to about 100Hz), it should cause minimal interference within the MR environment because the power source is optical and inherently MR-compatible, and the currents generated are on such a minute scale and are internal to the molecular structure of the material. While the strain of each individual bimorph is likely quite small, they can be stacked, analogously to piezoelectric materials, to create larger displacements.

3.3 Musical Performance in MRI Scanner

Neuropsychological MRI studies involving musicians is a major area of interest in determining the neural correlates of musical composition, performance, imagery and listening. As with haptic studies, MR-compatible musical interfaces have evolved to approach their non-MR-compatible counterparts. Early MRI studies involving musical performance did not even use interfaces. In a study of violinists, subjects were asked to use their chests as the fingerboard and perform left hand movements only: shifting their hand to the proper

positions with their fingers properly spaced to approximate in-tuneness and tapping their fingers with the appropriate timing to simulate a note onset, all while a trained observer looked on [55]. Similar tasks for pianists include finger-thumb opposition sequences whereupon the subject touches the thumb to one of the four fingers of the same hand [51, 63]. Other studies have used a flat fibreglass board to provide a reference surface as to where the subject should tap as if they were playing a piano keyboard [5, 48]. Yet other studies have used an electronic piano keyboard stripped of its electronic and ferromagnetic parts to ensure MR-compliance [4, 46, 59]. While this type of interface provides the subject with a physical sensation closer to that of a keyboard with moving parts, its functionality as an electronic piano has been destroyed, and thus auditory feedback is not presented. It is important to note that all of the above interfaces (or lack thereof) do not provide any direct acquisition of behavioural data. The only ways that the experimenters measured subject performance in these studies was through direct or video observation. Direct human observation of the subject performing the task requires that the observer be present within the scanning environment throughout the scan. The observer may be able to determine gross errors in accuracy or timing, however they do not have the capacity to measure small scale movements and inter-onset-intervals. There is no possibility of secondary verification with direct observation as no behavioural information is stored, other than what the observer has written down or committed to memory, and this system is thus prone to error. Live video observation removes the observer from the scanning environment to the control room but does not improve data collection unless the video feed is also recorded for offline analysis. Offline video analysis may allow the experimenter to discover information they may have missed on the first or even second pass, perhaps even determine average movement velocities by tracking frame-to-frame displacements, however very quick movements will not be captured with normal video equipment, and time resolution will be limited

by the standard $25\text{-}30Hz$ video frame rate. Computer-based video recognition tools may speed up this time-consuming process, however they would require the neuropsychology department to have the resources, funding, and graphics expertise needed to accomplish such an endeavour. Indirect behavioural assessments of this kind would be best solved using MR-compatible optical spatial measurement systems [75]. While electromyography (EMG) has been implemented safely within the MR environment, it has been employed mainly to ensure the subject is not moving a particular muscle during certain tasks or throughout part of a task [38]. EMG, while successful in measuring the excitation of muscle fibres, is unable to easily piece together the global compound movement from its constituent action potentials, and is thus not a reliable measure of accuracy, though it could be used for timing and measuring relative muscle flexion intensity.

Other studies involving musical tasks do not require interfaces that emulate musical instruments. Rhythmic tasks are a good example where a button response box, computer keyboard, or mouse are sufficient. In these cases however, it is important that the behavioural data (usually the timing of key or button onset and release) be recorded and synchronized with the stimuli. The study by Penhune et al. employed a computer keyboard with which subjects responded to the rhythmic stimuli in a $1.5T$ scanner, though there is no mention of specific MR-compatibility testing or specially-designed interface [65]. An MR-compatibility test of two commercially-available computer keyboards was completed by James et al. in a $3T$ head-dedicated scanner using a glass phantom, and found that two of the keyboards had decreases in the temporal SNR of 10% and 48% [47]. They go on to note that field homogeneity might decrease if the interface were brought into the bore of a whole-body scanner. Another rhythmic motor study by Chen et al. used a computer mouse as an input device for the subject to tap along with an auditory stimulus [15]. No information is given as to the compatibility of the mouse, only that the pneumatic head-

phones used to present the stimuli were MR-compatible. While this study was conducted in a $1.5T$ scanner, later studies conducted by Penhune et al. in a $3T$ scanner revealed that the electrical signals of the mouse were being corrupted by the MR environment and the interface ceased to function properly [70]. Upon discovering this, we set out to design an MR-compatible two-button response box, in the form of a computer mouse, which is detailed in this manuscript.

While many MR-compatible interfaces have been designed for robot-assisted surgery and neuropsychological haptic studies, there have been relatively few specially-designed MR-compatible musical interfaces. Details of the interfaces designed as part of the project presented in this thesis were published during the summer of 2007 [40]. More recently an MRI-compatible plastic MIDI piano keyboard, sporting 35 full-sized keys, was used in a jazz-style piano improvisation task [54]. Unfortunately, the article does not comment on the sensing technology, mechanical mechanism, nor on the feel of the keyboard or its ability to measure key strike velocities. The keyboard allowed the experimenters to directly detect note and timing of each key played in order to provide auditory feedback as well as logging the information for offline-analysis. The keyboard was placed on the lap of a patient lying supine inside the bore of a $3T$ scanner.

3.4 Summary

In this chapter we looked at various MR-compatible sensing and actuation techniques, as well as several MR-compatible interfaces for both musical and non-musical tasks. Optical sensing, due to its inherent immunity to EMI and wide variety of possible applications and implementations, makes it an ideal candidate for incorporation into MR-compatible devices. Table 3.1 summarizes the techniques and possible applications of common optical

sensing methods.

Modulation type	Interrogation technique	Advantages	Applications
Intensity	Direct or differential sensing	Simple to implement	Position measurement, quadrature encoding
Polarity	Polarizing filter	Facilitates rotational measurement	Angle measurement, magnetometer
Phase	Interferometry	High sensitivity to displacement	Seismometer, path length measurement
Frequency	Reflectometry and interferometry	Ability to embed within optical fibre	Strain gauge, temperature sensor

Table 3.1 Optical sensing guide.

The research of MR-compatible actuators is a growing field and will only continue to grow as these tools and techniques are applied to robot-assisted surgery, human-implantable devices, and interfaces for neuropsychological studies. Table 3.2 summarizes the MR-compatible actuator types we explored.

We also discussed the motivation for electronic collection of behavioural data, especially when considering the adjudication of musical tasks. In the next chapter, the prototype specifications and design methodology are presented, detailing interface interaction and behavioural measures to be culled from the musical tasks. As well, a technical description of the prototype implementations is provided.

Technology	Description	Advantages	Applications
Piezoelectric	Deformable crystal under electric field	Low current, high speed	Ultrasonic motors
Hydrostatic	Pistons transmit forces through system of fluid-filled tubes	Large forces, no electronics	Master-slave configuration for remote surgery
Electrorheologic	Fluid with electric field-dependent viscosity	Electronically-controllable material property, low current	Passive actuation as a brake
Electrostrictive	Deformable polymer under electric field	Low current, stackable, binary operation	Resizable MRI head coil
Electrostatic	Forces created across charged parallel plates	Low current, standard micro-fabrication process	Linear three-phase motor
Electromagnetic	Forces created through interaction of electrified coil and scanner's magnetic field	Large forces, high speed	Torque generator, vibrotactile device
Photostrictive	Photon-deformable bimorph	Optical power source, stackable	To be explored...

Table 3.2 MR-compatible actuator guide.

Chapter 4

Interface design

This chapter deals with the design constraints, initial design approach, and implementation details of the first prototypes. Two interfaces were constructed: an fMRI-compatible electronic piano keyboard and an fMRI-compatible two-button response box in a computer mouse form factor. Detail will be focused on the piano keyboard, as the mouse was derived from the former.

4.1 Design constraints

This thesis lays out the design for two different interfaces for use in fMRI experiments: an electronic piano keyboard and a two-button response box resembling a computer mouse. Both the piano keyboard and the response box were designed to be used during fMRI scanning in a $3T$ scanner at the Montreal Neurological Institute (MNI). The devices were to be MR-safe and MR-compatible. MR-compatibility for our purposes was defined as a device which functioned properly inside the scanner while actively scanning and did not create any image artifacts during an anatomical or functional scan. Spatial measurements

taken of the scanner environment constrained any device brought into the bore to a width not exceeding 54.5cm , and cabling between the interface and a host computer to no less than eight metres in length to reach the isolated control room outside of the MR environment housing auxiliary equipment. The interfaces were to provide electronic communications with a host computer for data logging and synchronization of stimuli and feedback. The interfaces were meant as initial prototypes to show proof of concept and were not meant as final products. While perhaps not optimized for cost, the interfaces were to be constructed on a minimal budget. Minimal time in the scanner was allotted for testing, therefore the designs were approached with a goal of designing interfaces that were theoretically MR-compatible and not approached in an empirical “test and refine” manner.

4.1.1 Piano keyboard design parameters

The piano keyboard was to be used in fMRI experiments, including one- and two-handed rhythmic, harmonic, and melodic piano tasks. Subjects were to include professional and novice players, so special emphasis was given to the touch and feel of the keyboard, especially that it should remain as true to its acoustic brethren as possible. A goal of twelve standard size keys was the original target, in order to give a one octave span. The keys were to be weighted as opposed to spring-rebounded, though a proper piano action was deemed useful but unnecessary, and likely not feasible in the small confined space of the scanner. The keyboard was to be mounted on a movable fixture to allow for individualized positioning, however the keyboard would be placed at arms length from the subject’s head and would not be placed in the imaging volume. True polyphony was required such that each key’s press and release could be sensed individually and independently. Key press velocity and force sensing was also on the initial list of design constraints, however it was decided that average key velocity near the end of its travel was sufficient to determine

what would be equivalent to the hammer-string force of an acoustic piano. Key velocity was to be used as a behavioural measure and as a means to modulate the amplitude of auditory feedback. While an oft debated subject [33], distinguishing between struck and pressed piano key onsets was not germane to our proposed research goals. Isometric force measurements, such as aftertouch on electronic keyboard-based synthesizers, as well as key acceleration and position profile measurements were discussed, but were omitted in the primary design constraints of the initial prototype, though possible sensing techniques are briefly discussed herein. No sampling rate nor resolution specifications were given for key sensing, however in order to create a faithful piano emulation, the device must give the appearance of real-time playability and a full dynamic range. It was required that the sensing data be conveyed to a host computer using a standard communications protocol in order to facilitate data logging, synchronization, and real-time auditory feedback. Auditory feedback would be presented in real-time using MR-compatible dynamic headphones, with sounds synthesized onboard the device, using a separate synthesizer, or on the host computer.

4.1.2 Computer mouse design parameters

The computer mouse-like response box developed as part of this project was intended for fMRI rhythmic tapping or clicking tasks. It was found that the computer mouse that had been functioning inside the 1.5T scanner for the aforementioned purpose did not function properly inside the 3T scanner during imaging due to induced electromagnetic interference [70]. The mouse that was being used was free of ferromagnetic parts, however in all other ways it was a standard commercial electronic computer mouse connected to a host computer, with no special measures in place to ensure MR-compatibility. The mouse was used for the sole purpose of extracting button press and release timing information. All other

data, including spatial positioning, were not of interest.

Symbol error manifests when induced noise from the scanner is superimposed on the signals emanating from the mouse — which represent and communicate button presses — and causes the host computer to misidentify certain encoded signals, known as symbols, by adding to (or subtracting from) their nominal waveform. A computer keyboard connected to a computer undergoing this type of malfunction might generate random letters in an idle state, and randomly misinterpret typed characters, leading to a log of meaningless data. In the case of the non-MR-compatible computer mouse operating in the $3T$ scanner, spurious symbols were being created and interfered such that authentic and relevant symbols, being misidentified due to symbol error, were lost.

An attempt was made to replace the flawed computer mouse with a commercial fibre optic-based MR-compatible response box. It was found, however, that the response box available at the MNI did not transmit a button release transition symbol.

The goal of designing an fMRI-compatible computer mouse was to endow the experimenter with the ability to record button press and release timing and velocity information, in the absence of scroll wheel and position tracking functionality. The purpose of using the computer mouse form factor, for what was merely a two-button response box, was to recreate the ergonomics of the computer mouse that subjects were using for training of behavioural tapping tasks outside the scanner. The constraints of the mouse were similar to the piano keyboard, but on a much more basic and general level. The touch and feel of the mouse buttons were to be maintained across experimental setups to provide subjects with a similar experience during learning and testing phases. The mouse was to be mounted on a fixture having a flat surface to stabilize the mouse in the scanner and provide support for the subjects' forearm and wrist. The mouse was to communicate electronically with the host computer using a standard communications protocol in order to facilitate data logging,

synchronization, and visual stimulus and feedback. The two-button response box was to sense individual button presses and releases independently, providing as well a measure of the average transition velocity. The design was further constrained by a paper-to-prototype time-line of under three months, and all with a minimal budget and testing time within the MR scanner itself.

4.2 Design paths

This section details the design options that were considered for each interface and interface subsystem. Included, as well, are possible approaches to various subsystems that were not implemented on the first prototype but may be of use to future prototypes and devices. The bulk of the fMRI-compatible two-button mouse design was derived from the piano keyboard prototype, and as such, detailed information pertaining to both devices will appear within the piano-related sections only.

4.2.1 Piano keyboard overview

The fMRI-compatible piano keyboard was divided into four basic subsystems: the mechanical interface, the data acquisition subsystem, the processing layer, and the communications module. The mechanical interface is the physical structure which includes the keys and keybed. The data acquisition subsystem is responsible for transducing mechanical actions into electronic signals. The raw electronic sensor data is translated in the processing layer into a usable data set representing the user's tangible interaction with the interface. The communications module enables the transmission and reception of data between the processing layer and the host computer. Each subsystem was essential to the overall design, however each subsystem could be implemented and tested in absence of the others. It is

this modular design process that guided this project and can be seen throughout.

Mechanical interface

The physical design of the piano keyboard prototype was meant to mimic that of an acoustic piano keyboard. The first decision that was made was to determine the type of key rebound that would be used: either spring, elastic, or counterweight. The main problem with the spring or elastic rebound system was how it would feel to the pianist as they depressed a key. We can approximate the force interaction with a spring-loaded key as

$$F_x = kx$$

where the force needed to displace a key, according to Hooke's law is F_x and is proportional to the displacement of the key through a distance x scaled by the spring constant k . Thus the force pushing back on the pianist's finger increases linearly (as we model the spring as linear) as the key is depressed, making it easier to depress at the beginning of its travel than at the end. (This analysis ignores for the moment that this system is actually a second class lever, and that the restoration force at the finger-key contact point depends on its position with respect to the fulcrum.)

Whereas an acoustic piano key, without the action in place, uses counterweights to restore a depressed key to its rest position and can be approximated as

$$\tau_\theta = l_m mg \sin \theta$$

where τ_θ is the restoring torque of the key moved through an angle θ , with distance l_m between the counterweight of mass m and the fulcrum, and constant acceleration due to gravity of g . This excludes the mass inherent in the key, as we can assume that it is small

compared to the mass of the counterweight and that the inherent mass of the key on one side of the fulcrum cancels that of the other side. The restoring force F_f at the point where the pianist places a finger can be approximated by

$$F_f = \frac{F_m l_m}{l_f} = \frac{m g l_m}{l_f}$$

where F_m is the force of gravity due to counterweight and l_f is the distance between the fulcrum and the finger. It is important to note that while the force at the finger can be tuned with the key length and relative placement of the counterweight, fulcrum and finger, as well as the counterweight mass, the restoring force is constant for a given key press and independent of its displacement.

What is missing from the above analysis are the frictional forces that are inherent in the movement of the piano key. While playing loud musical passages on the piano, the frictional forces are easily overcome and might be ignored; for pianissimo sections, however, this is not the case. The frictional forces in acoustic pianos result from the metal pins rubbing against the wooden keys, which is mediated by strips of felt within the mortises of the keys. It is this frictional force coupled with the restoring force that affords the pianist the ability to express a piece of music using a large dynamic range. Due to the fundamental difference in haptic feedback, it was decided that a weighted keyboard, and not the elastic spring-based keyboard seen in many commercially-available electronic clavier-based synthesizers, was to be used in the design of the fMRI-compatible prototype.

The piano action, the complex mechanism that transfers the motion of the keys to the strings, is not easily modeled in this fashion, and while it is an important part of the touch and feel of a piano keyboard, it was decided early on that it would be omitted from the first prototype due to space constraints and design complexities. Since the prototype

was to provide electronic and not acoustic auditory feedback (which would be infeasible within the noisy MR environment) the piano action was not required for its stated purpose. The pianist receives tactile feedback from the modern dual-escapement action through the keys of the keyboard (due to the added forces from the hammer on the back check and lever body, and forces from the damper lever), and while it might affect the feel of the keyboard, performance technique was thought not to be appreciably affected by this omission. Practiced pianists are quite adept at adapting to new keyboards as they do not have the convenience of porting their own instrument to every performance venue and practice room, and so our setup would not pose too much of an obstacle to the task at hand. As the interface was to be played in an MRI scanner, it was postulated that the subject lying supine, the keyboard above their lap in a dark confined cylinder, with their head encaged in a coil playing the piano with the claxon of the scanner in the background all the while, would not be overly concerned with the lack of a properly regulated action. Sensing of key presses, which will be discussed in the following section, from an auditory feedback perspective, would most authentically measure the terminal velocity of the hammer just before it strikes the piano wires. As all the energy imparted into the system is transmitted to the hammer by the key, it is reasonable in a simplified system to measure the terminal velocity of the key just before it hits the front rail at the end of its travel. On an acoustic piano, however, different types of key presses incur different key-hammer velocity and acceleration profiles [3].

In order to produce a keyboard with the above goals, a few options presented themselves: a keyboard could be acquired and modified to our specifications, or one could be built from scratch. Without the proper tools, funding, expertise, or time, building a keyboard from the ground up was not quite feasible. A weighted electronic keyboard could be purchased, but at a considerable price and requiring significant modification, whereas Montreal Piano

was kind enough to donate part of a keybed and keys from a near-century-old upright piano which, while not perfect and led to many headaches throughout, provided a solid starting point for the first prototype. The fixture upon which the interface was to be mounted is discussed in Section 5.2.2, however it was decided that its design and construction would be outsourced.

Data acquisition subsystem

There are myriad methods by which to sense the interaction between a pianist and a piano. Terminal key velocity was the value of interest, however the many approaches to that end and a mind toward future development meant a thorough review of sensing techniques. Included here is a parsing of applicable sensing technologies. It should be noted that the sensing system would be comprised of components contained within the MR environment as well as connections made to the processing layer kept outside of the MR environment in the control room. The signals from the transducers must be transmitted into the control room to conditioning circuitry (such as a preamplifier) as part of the data acquisition subsystem and, if applicable, active devices must be powered through conductors spanning the distance between control room and interface.

One might select to make discrete measurements or continuous ones. In so doing, one might wish to aggregate several samples as an average or plot the profile as a function of time or position. While the piano hammer-string interaction is dependent on the terminal velocity of the key (as well as felt compressibility and hammer shank flexibility), and while we wanted to capture discrete key press and release instances for synthesis purposes, ancillary behavioural data may be of interest to researchers, especially how these measures change with learning and mastership. As well, having a continuous measure of key position, for instance, through the full extent of its travel, enables the measurement of velocity or

acceleration by taking time derivatives (or differences if we first time-sample the data as is done with digital signal processing) of the positional information. Instead of sensing if a key is fully depressed or not by using a simple discrete sensor, one may use a continuous sensor and, with thresholding, determine not only when the key was pressed and released, but what happened before, after, and in-between. Measurement of force, specifically the force with which a finger presses a key and the force with which the key impacts the front rail, can be used to infer the acceleration and terminal velocity of the key (as the key's mass does not change as a function of time and none of the materials are particularly compressible or elastic). The finger-key force profile is especially useful for distinguishing between struck and pressed key strokes, and a derived measure of efficiency may correlate with factors such as confidence and mastership.

The multitude of electromechanical transducers, specifically those capable of transferring mechanical action into electronic signals, makes choosing an appropriate technology and package an endeavour of its own. Measuring velocity directly, perhaps through ultrasonic Doppler shift, is difficult and not well-suited to the noisy MR environment, therefore an indirect method is more feasible. In addition, velocity measurement alone would not lead to a simple solution in resolving the instant when the key is pressed or released. Electric field (or capacitive), magnetic field (e.g. hall-effect), piezoelectric, resistive (e.g. piezoresistive), and optical sensing technologies all exist in packages capable of measuring position, acceleration, or force in one way or another (that is, either directly or indirectly). There are definite issues with the application of capacitive and hall-effect sensors within the MR environment: due to the coupling of electric and magnetic fields, these are the most likely measurement techniques to interfere with, or be hindered by, the electromagnetic fields of the scanner. Piezoelectric materials are those which generate an electric charge when deformed. Many electronic drum heads use piezoelectric sensing to measure stick

strike timing and force. A change in applied force causes a change in charge, which, given the proper circuit implementation, can be measured more easily as a change in voltage. Conversely, the conductance of a force-sensing resistor varies with applied force. The latter has a frequency response down to DC enabling it to transduce static forces, whereas piezoelectric sensors have a high-pass filter response. Both of these types of devices can be operated using relatively low currents, making them possible candidates for the MR environment. While they may have a negligible effect on the MRI scanner such that they do not degrade image quality, these types of sensors require conductors to be strung along some non-negligible length, increasing the probability that the scanner might affect sensor signal quality. Shielding the cable runs, and even shielding the sensors themselves, will help to mitigate induced electromagnetic interference. There is no guarantee, however, that an interface with this type of implementation will work properly without an iterative *in situ* test-and-revise design approach (which incurs considerable costs for scanner usage and marked time investment by technicians and designers). Compounding this, even if the device works in one configuration, a slight change in the orientation of the long run of cable between the scanner and the control room or a migration to a higher-field scanner may have significant repercussions. Patient safety comes into question when long conductors are brought into the scanner for several reasons. The first hazard, which is easily circumvented with optoelectronic decoupling of the voltage mains and sensor signals, is a usual one encountered in biomedical devices: risk of electric shock, especially from high-current surges. Isolation of the patient from the municipal power supply is mandatory for electronic medical equipment. Other hazards which could result in burns are RF heating of the sensing element, heating of an accidentally looped cable, or closing a circuit with the subject as one of the completed pathways. These dangers, while serious, can be averted with proper insulation and diligence. Due to the time and resources needed to sufficiently prove that

the piezoelectric or resistive sensors implemented in a design are MR-compatible, it became clear that these technologies while feasible, may not be optimal in this context. Optical sensing on the other hand poses no threat to the subject and obviates conductors and the need for shielding inside the MR environment. A basic optical sensing setup consists of a light source (which may or may not contain frequencies within the visible spectrum), a fibre optic cable, an optical modulation mechanism, a fibre optic return path, and an optical receiver. The emitter and receiver can be placed in the control room so that the electronics are isolated from any infringing fields, while the light is transmitted to and from the MR environment along fibre optic cables. Photons can be transmitted along fibre optic cables over large spans without signal degradation, even within the electromagnetically-volatile MR environment. Visible light corresponds to a wavelength of approximately $400nm$ to $700nm$, while the RF energy of the scanner has a wavelength of approximately $2.34m$, thus they can be separated very easily and do not interact. Photons are launched toward the optical modulation mechanism which imparts some variation upon them before they are transmitted back to the receiver. This variation can manifest as a change in light intensity, polarity, phase, or frequency and may represent a measure of position, acceleration, or force (among others). Optical sensing is immune to induced RF interference, capable of high sensitivity, and can be compactly packaged, however this is often coupled with increased component costs, sensitivity to mechanical strain, and design complexity. The overriding factors of the keyboard prototype were safety and compatibility with the MR environment, therefore optical sensing was the prime candidate for the task at hand. Designing an optical subsystem which met our goals within the given constraints meant selecting and implementing a simple and cost-effective solution from the many available options presented in Section 3.1. The implemented optical subsystem is discussed in Section 4.3.1.

Processing layer

Regardless of the sensing method employed, the processing layer is required to extract key press and release instances, as well as terminal key press velocity. The processing layer needs to provide the communications module with a discrete trigger of the key press along with the terminal velocity, and then provide a key release trigger when the key is deemed to be released. There is of course some subjectivity as to when the key is pressed and when it is released. In emulating an acoustic piano, the key is considered pressed when it nears the end of its travel with a minimum velocity, and is considered to be released after it has returned partway back to its rest state. These thresholds are stated in a position-dependent manner, though given a key acceleration (or applied force) within a specific time span, it can be said with confidence whether or not the hammer would have hit the string with a sufficient impact to resonate audibly. The question remains with a force- or acceleration-centric sensing system, when exactly the system should give rise to a sound, as the key's acceleration profile of an acoustic piano will determine when the hammer is thrown from the key and how quickly it lands its blow. This again relates back to an in depth analysis of piano action physics [39], which we look to simplify for an initial prototype.

Continuous data obtained by the sensor subsystem needs to be digitized through sampling and quantization for digital computation and communication purposes. Profiles of position, force, or acceleration require streams of data, with samples representing sensor values at specific points in time. The conversion process from analog to digital signals requires specialized circuitry to accomplish such a feat: notably filtering and an analog-to-digital converter. This increases complexity, and in order to process acceleration or force data in the hopes of extracting velocity and triggering information, such circuitry is necessary. Conversely, by making decisions based on comparisons of the input signal with a

known reference voltage, we can simplify our processing if we can measure exactly when a transition from “less than” to “greater than” occurs as we will see later.

If we were able to measure key acceleration exclusively, velocity would be derived by integrating the acceleration over the whole trajectory. Integrating once more and we can determine the position. These measures assume there is no initial velocity or positional offset, the shortcoming of which is that errors can creep into our system, thereby causing erroneous measurements. For example, after several key press and release cycles, a positional offset may accrue, and if we are using key position to determine when to take a snapshot of the velocity, then the velocity which is likely changing very quickly may be reported earlier than it should, representing the velocity not near the end of the key’s travel but at some point prior. In another approach, reporting the velocity, thus instantiating a key press, might take place upon a change in sign of acceleration (when the key starts to decelerate) and the release reported upon the commencement of deceleration in the other direction. There is of course a fallacy in this approach as we assume that the velocity profile is monotonic, which is not always the case.

Measurements exclusively of finger-key or key-keybed force will also provide suboptimal results. First, with finger-key force measurements, offset errors may arise as was explained above when integrating to determine velocity and position, simply because the force applied to the key is proportional to its acceleration (Newton’s second law of motion). Second, ambiguity arises between pressed and struck key strokes: the force profile of a pressed key will peak at the bottom of the stroke when the key hits the front rail, creating an isometric force measurement; whereas the force profile of a struck key will contain a local maximum at the beginning of the stroke when the fingers impact the keys and perhaps again if the finger continues to apply pressure to the key when it reaches the front rail. A similar problem arises if the force measurement is taken betwixt the key and the front rail: the

pianist can vary the pressure on the key once it has reached the full extent of its travel by “digging in” to the key, and thus it would be difficult to differentiate a note played forte by throwing the key down and a short note played mezzo piano effected with a substantial isometric “aftertouch” force. Though we may not know which force to report, this setup will allow us to easily determine whether or not the key is fully depressed. Using both force sensors at the same time, one between finger and key, the other between key and keybed, would help to remove the ambiguity in determining key stroke type.

Measuring key position exclusively enables a reconstruction of a key’s velocity profile by performing a time derivative or sample-to-sample difference operation. If the velocity needs to be reported at only one location, only the time difference between two closely-spaced points is required. The same setup can be used to determine key release timing and velocity by taking measurements when the key travels in the opposite direction. This time-derivative approach does away with the source of aggregate error found in the integration-based formulations by making use of stationary spatial references.

A more complex model of the acoustic piano, taking into account the variability in the delay (and order) between the key hitting the front rail and the hammer hitting the string when considering pianissimo and fortissimo dynamics [2], can be accomplished by processing the information collected by key position, key acceleration, and key-keybed force. This would allow for a sliding-scale of note onset timing for notes played with different dynamics, as well as capturing key press information when the keys are “thrown down” without them hitting the front rail and thus differentiating between key stroke types.

Communications module

The last subsystem in the chain was the communications module responsible for transmitting key press transition and velocity to the host computer and/or synthesizer. Throughout

the design, testing, and *in situ* use of the prototype, the communications module took on different tasks. During the design and testing phase, much more information about the inner workings of the device was required than in the finished product. Therefore some flexibility in terms of connection type and protocol was warranted.

A distinction has to be made forthright between the electrical connection (known as the bus or interface) and the signaling method (or protocol). Certain protocols require specific electrical connections and those may be specified within the protocol standard. Other electrical connection standards allow for different signaling methods or symbol encoding while sharing common voltage levels, connectors, and pinouts. Serial protocols are standard practice when linking two electronic devices, especially when connecting peripherals to a computer. The three standard electrical connections that were surveyed are MIDI [60], RS-232 [72], and USB [18]. There are of course other standards such as Ethernet (IEEE 802.11), RS-485, and FireWire (IEEE 1394), among many others that would have sufficed, but simplicity, ease of implementation using available integrated circuit (IC) technology, and downstream connections narrowed the field. The design constraints do not require the data being sent from the prototype to the host computer or audio synthesizer to be particularly high-resolution and high-speed. MIDI and USB standards have specified electrical connections and protocols, whereas the RS-232 connections (known as serial ports on some now-aging computers) can transmit custom-encoded data packets using designer-specified data (or baud) rates. While USB has several standard data rates, the slowest being $1.5MB/s$, MIDI is fixed at $31.25kB/s$. MIDI has the main and exclusive advantage of interfacing directly with most electronic music synthesizers. Using MIDI as our worst case example (RS-232 can be operated at baud rates lower than $31.25kB/s$, but there it serves no benefit in our implementation), we can calculate the transmission latency for real-time auditory feedback when triggering synchronously played notes. The number of

bits required using MIDI messaging to convey a single “note-on” event (or key press in the terminology used previously) is thirty bits. For every byte (or eight bits) of actual information, two bits, the start bit and the stop bit, are used as bookends. The note-on message is made up of three bytes: the first is a status byte containing the channel number, the second byte represents the note number corresponding to a given pitch, the third byte conveys a seven-bit note velocity corresponding to the note’s dynamic level. Looking at the end-user specifications, we assume that the prototype has a maximum span of two octaves, or 24 keys able to be played simultaneously for true-polyphony. This translates to 30 bits for each of the 24 keys at a baud rate of $31.25kB/s$, giving a transmission time of,

$$t_{transmission} = \frac{30_{bits/key} \cdot 24_{keys}}{31250_{bits/second}} = 23.04ms$$

which is perceptually small enough to call “real-time” and well below the $270ms$ delay time for maximal delayed auditory feedback response in keyboard tasks [23, 28]. This calculation does not take into account the time needed for preprocessing of sensor data and synthesis, however it is unlikely that the task would require all 24 keys to be played at once.

Another advantage of using the MIDI messaging protocol is that it allows for custom system-exclusive messaging, allowing for extensibility such as higher resolution velocity representation. While the MIDI standard specifies its own electrical connection, MIDI messages can be sent over RS-232, and using standard ICs or converters it can be used to communicate with a software synthesizer running on a host computer. Data encoded as ASCII can be sent over RS-232 to a host computer at higher-than-MIDI baud rates; accomplished similarly with USB using application-specific serial data converter ICs. These higher data rates allow more information to be sent in a given period of time and are suitable for higher-resolution data streams and debugging, though as we’ve seen are not generally

needed for control of basic sample-based synthesis common to MIDI synthesizers.

A final comment on the OSC communications protocol (for more on OpenSound Control see [81]) which was proposed as a replacement to MIDI. It has many advantages including: increased messaging efficiency, higher transmission rates, more varied and higher resolution data types, human-readable message naming conventions, and is generally more flexible. This flexibility comes with increased complexity, and the added features of OSC do not sufficiently offset the usefulness of MIDI, which will likely remain the standard for some time among electronic keyboards.

4.2.2 Computer mouse overview

The following section outlines the design approach to the mechanical interface of the fMRI-compatible two-button response box in a computer mouse form factor. The sensing, processing, and communication subsystems are identical to those of the keyboard, with the exception of sensor mounting which will be discussed further on and in more depth as part of the design implementation section. Thus the same information will not be reiterated here and the reader is asked to refer to the previous sections for details relating to the aforementioned subsystems.

Mechanical interface

The specifications for the MR-compatible computer mouse were little more than a two-button response box enclosed in the shell of a computer mouse. As far as positional and scroll-wheel information common to computer mice, these were not part of the design and were specifically not desired. The primary objective of the computer mouse, herein referred to as simply “the mouse”, was to determine the duration of button presses, specifically their onset and offset timing. The mouse was to be mounted on a stabilizing substrate for

ergonomic and motion-reducing purposes.

Two choices were apparent from the conception of the device: whether to build the interface completely from scratch or to modify a working computer mouse. Due to the time constraints and the availability of inexpensive mice, it seemed that the latter option would ease the construction of such a device. In starting with an actual mouse, the feel and form factor were already present, and without the expertise and resources to design and mold a plastic mouse look-alike it seemed ridiculous to proceed otherwise. The downside to using a pre-existing structure is the fact that the sensing subsystem must be adapted to the mechanical interface, while ideally both would be developed in tandem. The short travel of a mouse button (at most a few millimetres) meant an increased demand on sensor sensitivity and mounting precision. Button onset velocity measurement, while more of a secondary objective, would be subject to more error and variability than onset and offset timing.

Modifications would include removal of ferromagnetic components and internal circuitry, disabling and/or removal of unnecessary mechanisms and parts, sensor mounting, and securing the interface to a fixed base. The potential difficulty would be removing and replacing ferromagnetic mechanical parts that produce the button “click” (usually a mechanical switch) that is the basis for the tactile feedback required to maintain the feel of a computer mouse. Rubber or plastic substitutes could be developed to enable a softer button click. A small switch containing paramagnetic materials that would have a negligible effect on field homogeneity, especially when positioned at arm’s length from the imaging volume, would be a more attractive alternative to retain the feel common to most computer mice.

4.3 Implemented design

In this section, the technical designs as implemented are presented. Again, the implementation of the piano keyboard and mouse vary only in the way of physical interface and sensor mounting (and thus sensor calibration). As such, all of the details will be presented in the clavier section, and only mouse-specific details will be presented in its respective section, omitting redundant descriptions.

4.3.1 fMRI-compatible piano keyboard design

Though the system was divided into four conceptual parts previously (i.e. the physical interface, the data acquisition subsystem, the processing layer, and the communications module), the implementation of the keyboard is divided into three parts: the physical interface, the analog and mixed signal electronics, and the digital hardware and firmware. Though the data acquisition subsystem, processing layer, and communications module are separate conceptual entities, they are realized in overlapping sections, such that some of the sensing and processing are implemented together, while the remaining processing and communications are implemented elsewhere. All of the design steps were first implemented on one key, then a set of three, and finally eleven keys were completed for the first prototype.

Physical piano interface

The weighted action-less keyboard was built from a quarter of an upright piano and modified to ensure MR-compatibility and to ready it for augmentation with optical sensors. The set of keys and keybed was saved from the kindling pile and salvaged from Montreal Piano, a local piano repair shop. Due to its age and state of disrepair, the keys were imperfect and nonuniform; some even stuck against others due to warping.

The first task was to remove all ferromagnetic parts, which included a few screws in the base of the keybed, small screws on each key which seemingly no longer served a purpose, as well as the back checks attached to the far end of each key via a metal rod embedded deep into the key. The screws were easily removed, however the back checks had to be removed by sawing off the far ends of the keys, as the rods could not be removed by force. The brass front rail and balance rail key pins, though metallic, were paramagnetic parts and were thus not removed. As the device would be placed at a distance significantly removed from the scanning volume, and as the pins were not in a loop configuration, it was inferred that they would not significantly impact image quality.

Next, the keys were filed down such that they would not interact with each other when depressed — due to warping, this unfortunately was the case with a few keys, likely caused by humidity and disregard. The tops of the keys were sanded, as the ivory had been removed and thus were in need of resurfacing. The keys were then re-weighted with lead shot for two purposes. First, the front of the piano keys were larger and thus heavier than the portion sitting behind the balance rail. Thus without the piano action forcing the back of the key down, it would naturally return to its depressed position, making playing impossible. Second, in order to provide a piano-like feel, the backs of keys had to be weighted to not only balance the keys, but to compensate for the loss of the force feedback as well. The keys were weighted with a maximum key-to-key deviation of $3g$ at the tip of each key. Lead weights were embedded in holes drilled into the back of each key, and glued into place. The available volume of the key was maximized while still maintaining its structural properties. The mean key weight was $45g$, somewhat on the light-end, but within the normal range of piano key weight.

While the weight of the key was sufficient, the feel of the keyboard did not have the appropriate dynamic frictional forces when played. Likely the felts within the mortises

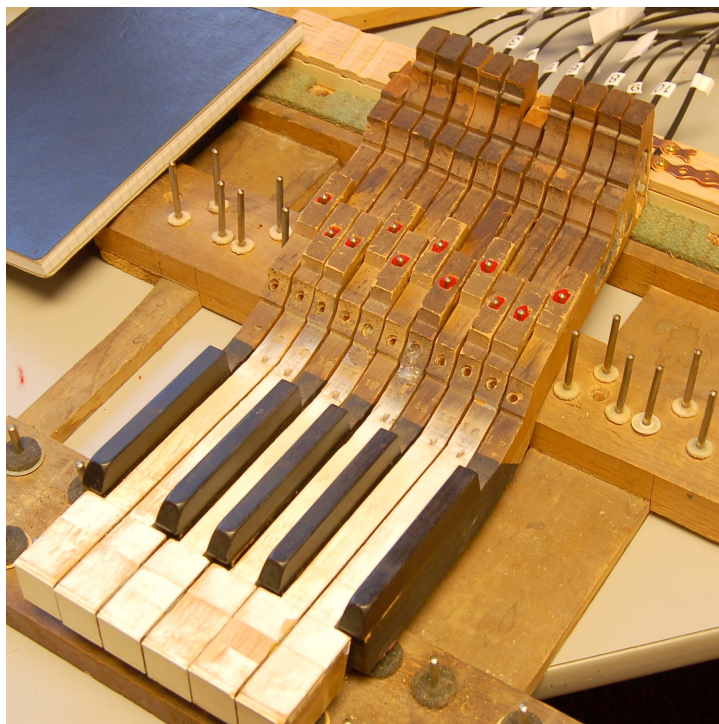


Fig. 4.1 Piano keyboard interface.

of each key were the originals as they were badly worn and no longer had any give or nap. Thereupon, the old felts were removed and replaced with new pieces glued to the inside of the keys. The new felt provided resistance to the balance rail pins while the keys were moved. In order to provide a uniform feel across keys, the felt was softened in the stiffer keys in a similar fashion used in needling piano hammer felts. Figure 4.1 shows the completed keyboard interface.

Aluminium-backed plane mirrors, measuring one square centimetre, were glued to the back end of each key near the bottom, as shown in Figure 4.2. The back of each key, and thus the mirror, moved vertically approximately three centimetre during a key press. Considering a single depressed key, the mirror reflected light launched down one optical fibre back toward a second fibre placed alongside the first. A more detailed explanation of



Fig. 4.2 Reflectors glued to key ends, with keys in varyingly-depressed positions.

the sensing mechanism is presented in the following section.

A wooden platform was added behind the back rail to which the fibre optic cables were secured, as seen in Figure 4.3. Strips of flexible copper strapping sandwiched the fibre optic cables to the keybed. While the copper components are conductive, they are non-ferromagnetic and would not reside within the imaging volume during scanning. The copper strips were fastened to the keybed with brass screws set between each cable pair. This allowed for the cable pairs to be adjusted independently of each other in order to optimize the distance and angle between the ends of the cables and the mirrors. The maleable copper strips had better fastening and fatigue characteristics than the wood and plastic configurations that were tested.



Fig. 4.3 Optical cables secured to the keybed.

Analog and mixed signal subsection

The analog and mixed signal subsection consisted of the sensing hardware and the logic elements used to extract key position information. The emitter type was a super-bright red (660nm nominal peak wavelength) LED with connector-less screw-type housing and integrated lensing made by Industrial Fiber Optics Inc. (part# IF-E97) [44]. The detector type was a source-matched wide-spectrum ($400 - 1100\text{nm}$ usable range) photodarlington transistor also housed in a connector-less screw-type plastic molding with integrated lensing (part# IF-D93) [43]. For each piano key a frequency-matched $980\mu\text{m}$ (diameter) plastic core duplex cable [78] was employed to convey light into the scanner using one core connected to the LED, while the other core was connected to the detector. Free ends were secured to the piano keybed and aligned with a reflector glued to a piano key. For each key, a fibre pair of 10m was used, with the whole set fashioned together with spiral-wrap plastic

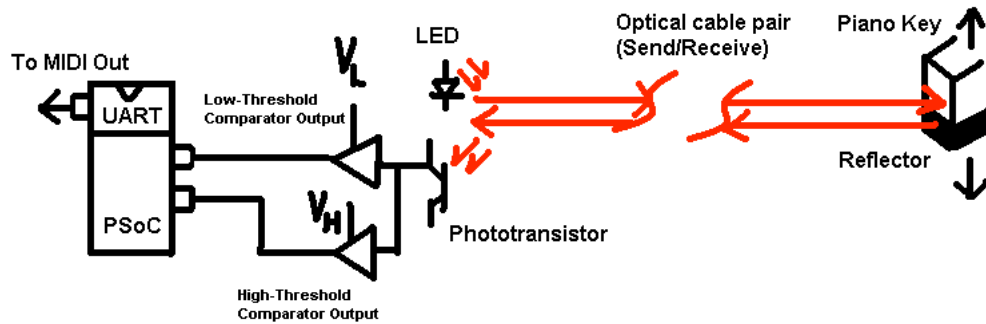


Fig. 4.4 Sensor subsection block diagram.

cable bundlers. The reflectors were one centimetre square, and were vertically displaced into alignment with the fibre pair when a key was depressed, efficiently reflecting most of the incoming light back toward the detector-connected cable. Upon key release, the back of the key would fall down, as would the mirror, causing the light spot generated by the LED to be absorbed and diffused on a non-reflective part of the key surface. The central idea was to reflect light from the source fibre into the detector when the key was depressed, and thus when the mirror was lifted into place. When the key was released and at rest, the mirror would be displaced and thus the light source would be absorbed and diffused by the unreflective end of the key. Please refer to Figure 4.4 for a block diagram of the sensing system, and Figure 4.5 for a picture of the entire circuit board.

The circuitry surrounding the emitter and receiver included the power supply, biasing resistors, comparators, and trim-pot reference generators, as seen in Figure 4.6. The power supply, which also supplied the digital section, was a simple 5V output DC-DC converter with appropriate decoupling capacitors. The biasing resistors set the LED current and phototransistor quiescent point. The phototransistor was wired as a simple common-collector emitter follower, with the emitter resistor adjusting the photosensitivity. Two comparators per key were implemented to provide binary outputs to the microcontroller (denoted as *DH* and *DL* in Figure 4.6): an output high (5V) if the input voltage was higher than

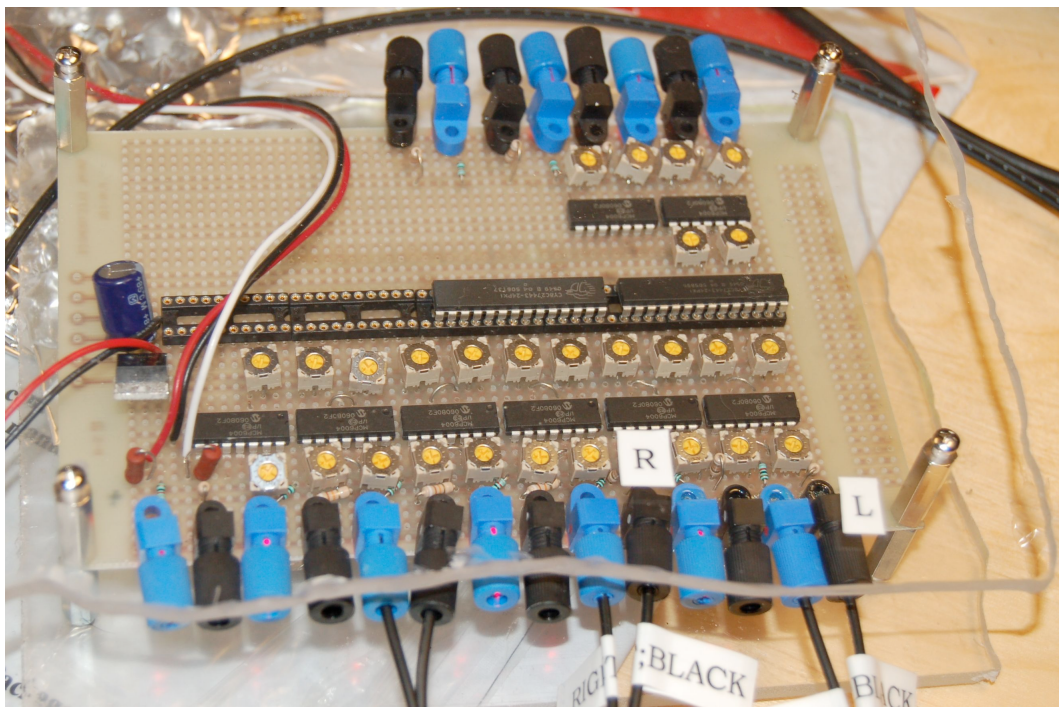


Fig. 4.5 Circuit board populated with signal acquisition and processing electronics.

At the bottom and top of the circuit board the photoemitter and photodetector connectors are visible, with three pairs of optical cables connected. The power regulator is shown on the left-hand side, with input power and communications cables. Comparators are surrounded by trim potentiometers, with the longer microcontroller ICs in the centre inserted into sockets.

the reference voltage, and an output low ($0V$) otherwise. The comparator reference values were set with potentiometers to different threshold levels representing key position: the low reference voltage (V_L) corresponded to a partially-depressed key, while the high reference voltage (V_H) corresponded to a fully-depressed key. For example, if the key were partially depressed and thus $V_H > V_{in} > V_L$, then DH would be kept low and DL would be pulled high. Due to key-to-key variations, these voltages were calibrated for each individual key to optimize transition detection and velocity measurement. As a key was moved into place, the analog sensor output voltage corresponding to the detected light intensity first rose slowly as the light was only partially reflected by the mirror and peaked when

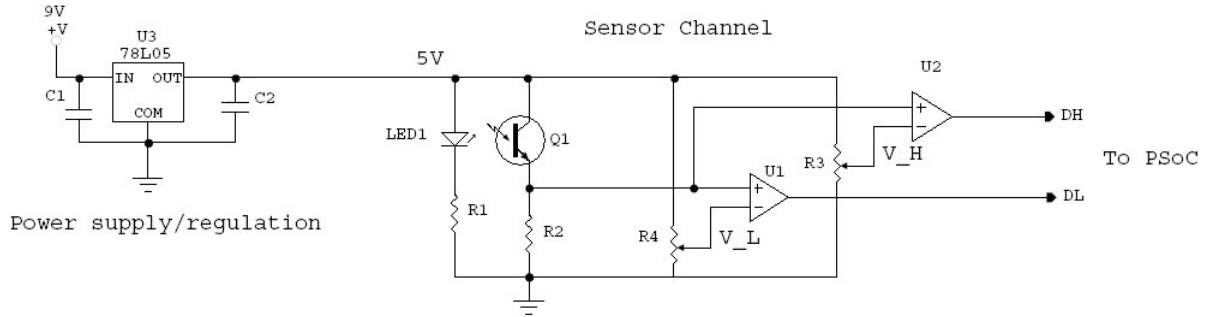


Fig. 4.6 Schematic of analog subsection with power supply.

fully aligned. Some ripple occurred in the signal during more forceful key presses, and so as to disambiguate single hard strikes from two very quick key strikes, V_L and V_H were separated by a significant voltage. The reason for this will become more clear as we move on to the next section detailing the key press acquisition and reporting. A single detector with one fibre optic cable pair and two comparators were used for each key, though two detectors with one comparator and fibre optic pair apiece would have also sufficed. The later implementation would, however, have incurred increased costs and taken up more space with the additional components. As well, additional variables, such as the difference in alignment between fibre optic cables of a single key, would have complicated the design setup and significantly contributed to increased calibration time.

Digital hardware and firmware

The digital portion was implemented on a Cypress Microsystems CY8C27443 [20] programmable system-on-chip (PSoC). The PSoC is a microcontroller core integrated with reconfigurable analog and digital hardware blocks such as amplifiers, filters, analog-to-digital converters, and counters, as well as a universal asynchronous receiver/transmitter (UART) block. The detection of key press transition and velocity, as well as the communications

module were implemented on the PSoC in C and assembly programming languages.

Comparator outputs were wired to “change-from-read” interrupt-enabled input pins on the PSoC. Instead of continuously polling all of the input pins, any comparator transition fired an interrupt. The PSoC contained only a single general purpose input/output (GPIO) interrupt vector. Thus upon firing of the GPIO interrupt, the current state was compared to the previous state to determine which keys were in transit. A finite state machine was designed to distinguish between up and down transitions by comparing the new transition type with the previous state. Please refer to Figure 4.7 for a pictorial view of the state machine. As V_H was always at a higher potential than V_L , then DH was never high without DL also being high. There are thus three states, and two state variables representing the current state and transitions. The impetus for the state machine was to ensure that no false key transitions were reported when the key was only partially depressed or released, even if the GPIO interrupt was fired due to a comparator transition. The 0/0 state is the OFF or totally released state. 1/0 refers to the partially-depressed state, with the first digit representing the value of DL (in this case it is high), and the second digit representing the value of DH (in this case it is low). When the key is fully-depressed, both state variables are high. Key transitions are only reported when jumping from 0/0 to 1/1 (note-on) or 1/1 to 0/0 (note-off), through 1/0. If a key in state 1/1 were to drop to 1/0, and returned directly to 1/1, then no authentic key transition took place and none was reported.

In order to measure velocity of key transitions (both note-on and note-off), a timer starts counting when the state machine transitions from 0/0 to 1/0 (for the note-on case). If the state returns to 0/0 from 1/0 without jumping to 1/1, then the time is reset and starts again at the next transition to 1/0. Assuming a key transitioned from 0/0 to 1/0, and continued on to 1/1 directly, at that last transition into the fully-depressed state, the timer is stopped, and its value represents the key transition velocity. This value, a direct measure

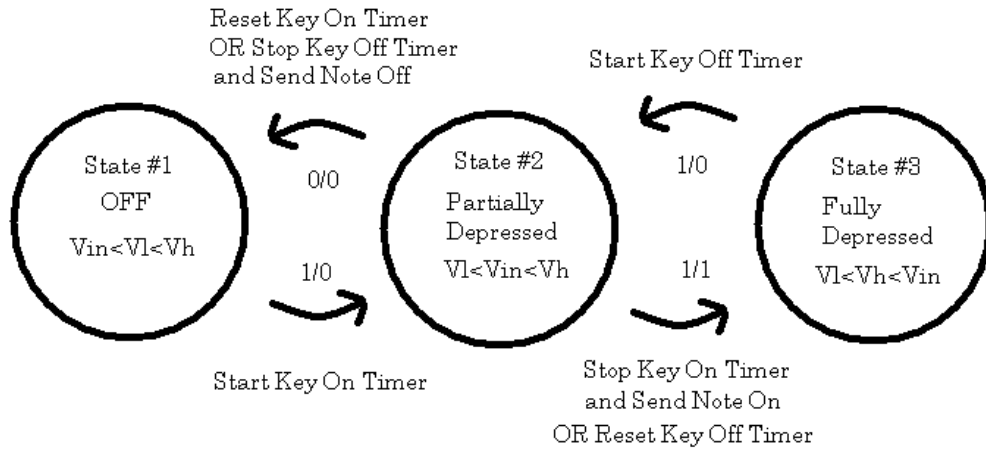


Fig. 4.7 Key transition state machine.

of transition time, was then mapped onto a velocity curve to obtain a MIDI-compatible velocity value from $0 - 127_{10}$.

Communicating key transition and velocity was accomplished with a UART block of the PSoC. For initial debugging purposes, a computer serial port was connected to the transmit (TX) line of the UART through a MAX220 RS-232 driver chip [57]. This IC level-shifted the $0 - 5V$ signal to the bipolar $\pm 10V$ signal that the RS-232 protocol required. Key number, velocity, and transition type was sent as ASCII data and received using Hyper Terminal at 115200baud , eight data bits, and no parity. For end-user purposes, the MIDI protocol was used, connecting the TX line to a 5-pin DIN connector. In this way, MIDI-compatible note-on and note-off messages were sent along with their respective key number and seven-bit transition velocity. These messages were natively understood by a MIDI-equipped computer or synthesizer for real-time auditory feedback. As well, system exclusive messages containing 32-bit transition time data were transmitted for logging and post-processing of behavioural data.

The 28-pin DIP PSoC chip, as implemented, could only accommodate seven keys, and

not the eleven augmented on the prototype. Therefore, the receive (RX) line of the UART was used to daisy-chain one PSoC IC to another. The TX line of one chip was connected to the RX line of the next, which fed through the MIDI data on available clock cycles. In order to avoid overlapping messages, each chip was associated with a different key number offset, providing distinct ranges. Conceivably, thirteen of these chips could be chained together to allow for 88 keys, however with increased latency for farther-removed chips.

4.3.2 fMRI-compatible computer mouse design

As stated earlier, the mouse design was derived from the keyboard prototype. The electronics were identical to those used in the keyboard, however two channels were utilized instead of eleven. As well, the threshold reference voltages were calibrated specifically for the mouse, as the travel and thus the sensor signal differential was quite small. What follows are the design details as implemented for the mouse, omitting a discussion of the electronics which can be found above.

Physical mouse interface

The fMRI-compatible mouse-like interface was built from a standard USB computer mouse, modified to meet the prototype specifications. The mouse was first gutted of all electronic parts, with the exception of the electromechanical button switches. The circuitry was removed as well as the wiring. The mouse ball, gears, springs, screws, and other internal mechanical parts were removed. The scroll wheel was glued in place so that it could not be turned. The mechanical switches were retained in order to maintain the well-defined “click” feel of the buttons. The switches were non-ferromagnetic, and the amount of paramagnetic material was quite small. Through the hole in the bottom of the mouse, where the mouse ball once protruded, a nylon nut and bolt secured the mouse to a wooden platform. A

rubber gasket ensured a secure mounting of the mouse to the platform without cracking the plastic mouse case. The gasket also eliminated any pivoting of the mouse on the platform.

Aluminum foil reflectors were glued to the exterior of the mouse buttons, vertically at the tips. Facing the reflectors, for each button a fibre optic pair was secured between wooden and acrylic panels with nylon screws and wing-nuts atop the main wooden platform. The wooden platform was countersunk on the bottom side in order to recess the nylon components. The ten metre-long fibre optic cable runs were housed in a plastic hose attached to the platform in order to protect the cables from being damaged if stepped on when installed in the scanner.

The reflectors were approximately 1mm in height and placed at the bottom edge of the movable portion of the button. The mouse buttons were vertically displaced approximately 2mm from total release to completely depressed. However, this distance changed depending on where, on top of the button, the finger was placed. In order to alleviate this variability, a tactile Velcro marker was placed on each button at a contact point optimized for maximal travel, where the subjects were to place their fingers. Figure 4.8 shows the mouse in use outside of the scanner.

4.3.3 Implemented optical force sensor

In addition to the optical position and velocity sensing detailed above, a simple optical force sensor was constructed using the same detector, emitter, and fibre optic cable pair. By cutting the sensing end of the fibre pair in a ‘V’-shape so that the core of one fibre was exposed to the core of the other, the amount of light coupled between the two fibres could be modulated by applying a force to the cleft. When at rest, the fibres are not well aligned and only a small amount of light passed from the emitter to the receiver. As the ends were



Fig. 4.8 Mouse interface.

pinched together, much more light was detected. The ‘V’ angle of the cleft determined both the force sensitivity and range, as more force is needed to bring the sides of a shallower cut cable together, while a deeper cut provided much less structural resistance to bending. A 45° cut seemed optimal for measuring gentle to moderate finger forces and saturated the detector output when fully pinched.

4.4 Summary

In this chapter we presented the design constraints, methodology, and implementation. The mouse-like response box design was derived from that of the piano keyboard, as all but the physical interface and the sensor mounting were identical. The keyboard interface was divided into subsystems: physical interface, data acquisition, data processing, and communications. Table 4.1 summarizes their implementation.

The following chapter details the testing of the prototypes, including calibration steps and *in situ* results. Recommendations toward improving next generation prototypes are

also presented.

Subsystem	Description	Inputs	Outputs	Implementation
Physical interface	Piano keys provide affordance for musical task	Human displacement of keys	Mechanical displacement of reflector	Modified wooden acoustic piano keyboard
Data acquisition	Sensing of key transitions	Reflected optical signal	Tri-state electronic representation of key position	Fibre optic cables, optoelectronic devices, analog hardware
Data processing	Extraction of key press timing and velocity	Electronically-encoded key position	Transition type and time of flight	PSoC interrupts and timers, state machine
Communications	Send MIDI data to host computer and/or synthesizer	Key number offset, time of flight, transition type	MIDI message with note number, velocity, and transition type	PSoC UART, daisy-chained for extensibility

Table 4.1 Review of keyboard subsystems.

Chapter 5

Device testing, calibration, and recommendations

This chapter elucidates testing and calibration methods, as well as device shortcomings and MR-compatibility. Recommendations to improve the first and next generation prototypes are posited.

5.1 Testing and calibration

In this section the testing of devices is detailed. Both devices were tested extensively outside of the scanner before being brought into the MR environment for pilot studies. While each subsection was tested individually to ensure proper functioning, presented below are tests of the interfaces as a whole. While there are commonalities between device electronics, testing of those will be presented first, followed by interface-specific details.

5.1.1 General testing

The electronics common to both the piano and two-button mouse-shaped response box satisfied the specifications. Upon key or button transition, the proper trigger was identified and reported with a velocity measurement to a host computer for logging and synchronization of real-time feedback. The electronic interface was connected to the host computer via a MIDI-to-USB M-Audio Uno. Using the integrated sound card and MIDI drivers of the host computer, latency was significant and in excess of $100ms$. Using instead an outboard synthesizer, auditory feedback was presented with imperceptible and negligible latency, well below $50ms$. Thus, as expected, the bottleneck was caused by software processing and not the control electronics. Transitions were sensed individually and independently, with no interference or delay caused by multiple simultaneous triggers. All transitions were sensed, no matter how quickly or slowly they occurred. All false triggers that were sensed and reported were caused by nonidealities in the physical interface, optical fibre-mirror alignment, or miscalibration. Velocity measurements were hampered by the same three parameters, and not the hardware or firmware.

Fibre optic cables secured to the interfaces were reconnected to the electronic control box at the beginning of each testing session and disconnected afterward. Of concern were the fibre optic interconnect terminations: the closely-spaced board-mounted photodetectors and photoemitters were difficult to use and upon disconnection and reconnection, calibration was often required. The board-mount nature of the optoelectronic devices, coupled with the forces required to connect and disconnect the fibre optic cables, meant that special care had to be taken to ensure that wear and tear was minimized. Slightly insufficient cable insertion depths caused significant optical transmission losses. Unfortunately, there was no clear indication when an optical fibre was insufficiently terminated inside the device

housing, and this led to much time spent debugging and calibrating.

5.1.2 Keyboard-specific testing

The piano keyboard performed adequately for most tasks. As only eleven keys were implemented, full two-handed playing was only feasible with overlapping hands, and tasks using this technique was shied away from due to concerns of creating complete conducting paths with the arms and torso through the hands. The feel of the keyboard was sufficient in weighting and damping to perform moderately difficult tasks, though the lack of a mechanical action was noticeable and belied the emulation. Key surfacing was less than refined, as were key-to-key nonuniformities arising from its age and humidity-related warping. Quickly repeated notes were achievable as was a wide dynamic range. False triggering was seen with very strongly struck keys, though due to the temporal proximity of the two reported strikes, false triggers were evident upon examination of the log file. Software routines implemented on the host computer mitigated erroneous production of real-time auditory feedback caused by false triggering. The device was sensitive to setup conditions and often required calibration upon reconfiguration. Figure 5.1 shows the photodetector output from a piano key struck five times within one second. The ripple at the peak of each key press results from the key's mechanical resonance when it hits the front rail, and lifts slightly at the fulcrum.

Keyboard calibration

With proper calibration the keyboard performed quite well. Calibration was required to set the threshold reference voltages and velocity mapping. The former was important for proper timing and limiting false triggering, while the latter provided a large dynamic range consistent across all keys.

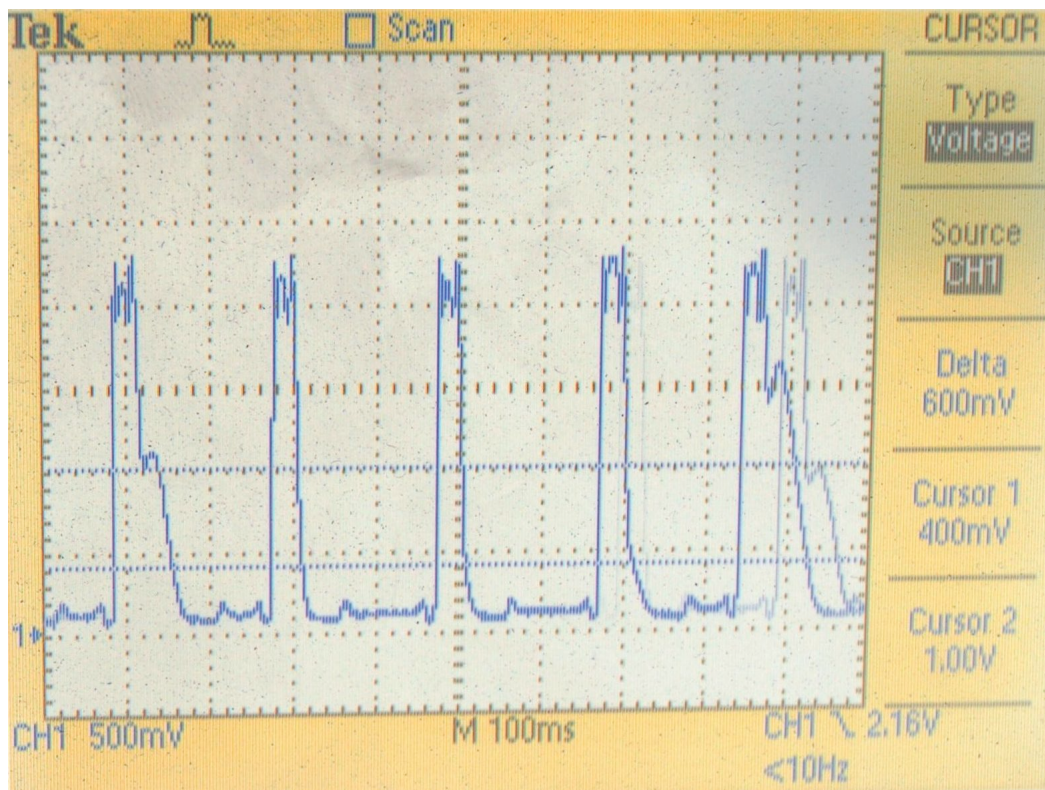


Fig. 5.1 Photodetector output showing repeated notes.

Calibration commenced with setting the high threshold voltage (V_H) to correspond to the end of the key travel. The low threshold voltage (V_L) was set to prevent false triggering though at the same time a compromise was made to allow quickly-repeated notes without fully releasing the key. This tradeoff was effective, however false notes were reported occasionally when a key was struck with great force causing the middle of the key at the fulcrum to lift off of the keybed, as detailed on page 41 of [39].

Velocity calibration was performed in two steps: an initial drop weight testing scheme, and a series of chromatic scales played at several different dynamic levels. Drop weight testing was accomplished by placing a weight, ranging in mass from 50g to 500g, at the tip of each key and recording the timing data to a host computer. These curves were extrapolated

and normalized to provide a uniform and appropriate dynamic range. However, small inconsistencies remained, causing nonuniform auditory feedback from one key to another for seemingly similar key stroke strengths. Thus, upon the initial laboratory calibration, a more pragmatic approach was laid: chromatic scales were played several times at *piano*, *mezzo forte*, and *fortissimo* dynamic levels and recorded separately, with special care made to use the same approximate key press force, with and without auditory feedback. The timing data was averaged within one key and dynamic level to smooth out accidentally hard or soft key strokes. A timing data-to-velocity curve was then created for each key and downloaded onto the chip. The scales and normalization were then repeated several times until the results converged and the adjustments made from one iteration to the next were indistinguishable.

Due to nonuniformities in inter-key travel, weighting and friction, sensor mounting, and reference voltages, each key had a different key press profile. Calibration attempted to mitigate those affects and normalize playing and feedback across keys. Slight shifts in sensor alignment and optical coupling from one setup to another caused, occasionally significant, changes in key press profile. Most of the difficulties were rooted in the mechanical construction (and wear) of the keys and keybed, causing secondary problems in sensor mounting and key velocity measurement which would not have occurred if the keys themselves were uniform. However, a usable and functioning electronic piano keyboard prototype was developed, in spite of the regular calibration it required.

MR-compatibility

As the electronics were relegated to the control room, as seen in Figure 5.2, and connected to the interface only in the way of fibre optic cables, the device was deemed MR-safe and MR-compatible *a priori*. The amount of paramagnetic material and its placement well

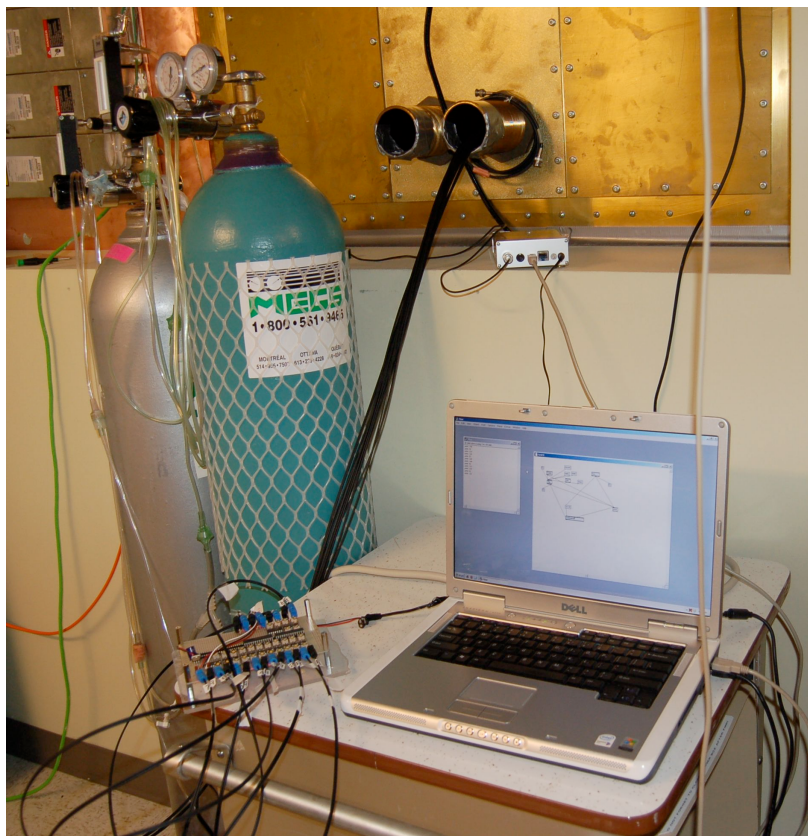


Fig. 5.2 Interface electronics in control room.

Fibre optic cables connect interface within the MR scanner to the signal acquisition electronics through the shielded port in control room wall. Interface electronics are connected to a host computer for data logging and control of auditory feedback.

outside the scanning volume during MR scanning sessions was considered insignificant and its effect on images negligible. Figure 5.3 shows the device being tested in the MRI scanner. Movement artifacts due to task performance are much more likely and significant sources of image degradation. As of this writing, SNR and field homogeneity tests have not yet been accomplished, though they are planned. Pilot studies inside with the MR environment have shown no image artifacts due to the device during anatomical and functional scans. As well, the device functioned properly, with the calibration caveats mentioned above, and thus performed no differently within the scanner than it did without.

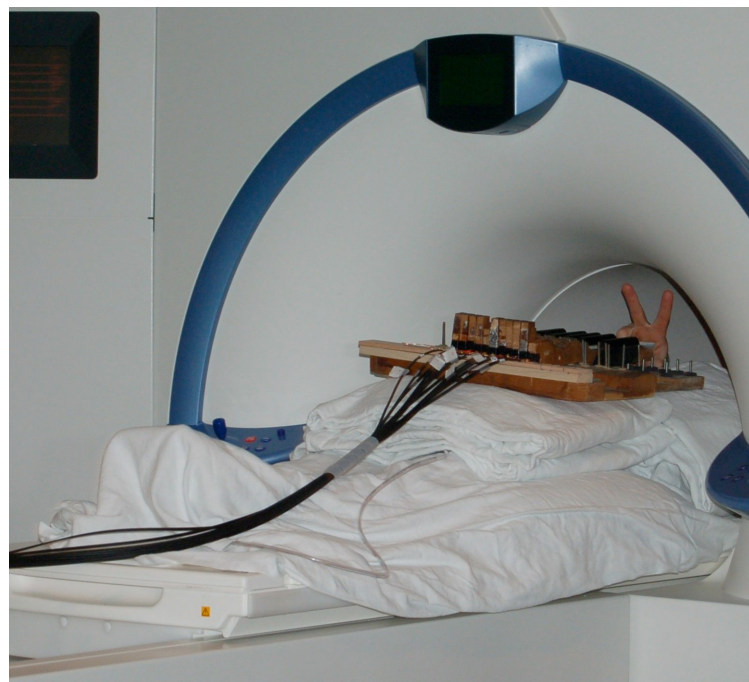


Fig. 5.3 Keyboard testing within MR scanner.

Figure 5.4 shows functional MR images¹ taken on the coronal, axial, and sagittal planes respectively, during a piano-playing task using the fMRI-compatible piano keyboard. The task included playing an eleven-note chromatic scale up and down two times with unrepeated upper and lower notes at a slow tempo (approximately 60-80 beats per minute), followed by a thirty-second rest period. This task was repeated eight times with and without auditory feedback. Scanning was done at the Montreal Neurological Institute's Brain Imaging Centre with images acquired using a Siemens 3T TRIO whole-body MRI scanner equipped with an eight-channel head coil and a T2*-weighted functional protocol (4mm isotropic resolution; 2.5s relaxation time; 30ms echo time; 256mm field of view; 90 degree flip angle; 64x64 matrix).

¹Courtesy of Christopher Steele, used with permission.

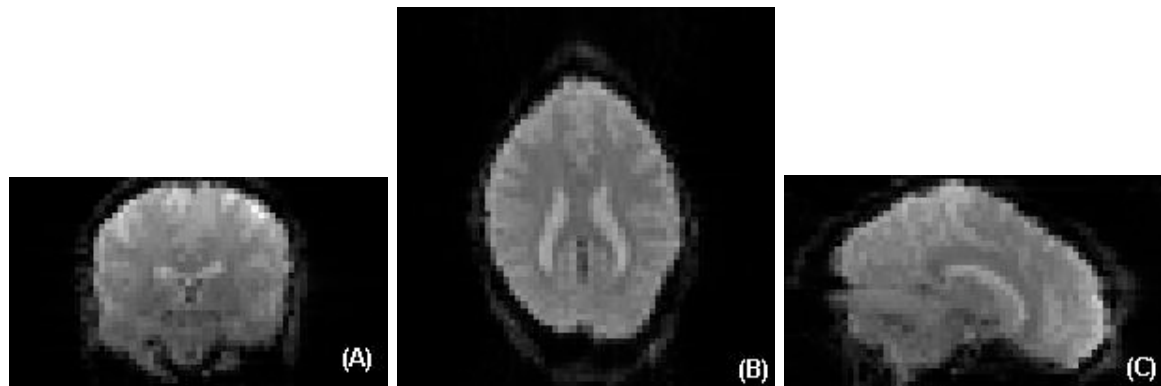


Fig. 5.4 Functional MRI scans with keyboard.

(A) coronal, (B) axial, and (C) sagittal slices of a subject playing the fMRI-compatible keyboard in the scanner.

5.1.3 Mouse-specific testing

The mouse-shaped two-button response box performed to specification when used as directed. Proper use meant that the contact point between finger and mouse button be located at the Velcro target. The tactile feedback was provided by the mechanical switch, however the actual sensing of button presses was performed at the button tip. Thus it was possible to actuate the switch without triggering a button press, and vice versa. The Velcro target was placed at a position such that the two events aligned as closely as possible. Strongly ballistic button presses and overly enthusiastic button releases tended to caused the button to oscillate and create false triggers. A strong ballistic button press followed by an immediate release was the worst case, often causing false triggers. Auditory feedback was not presented using the mouse, so false triggering was less of a hindrance than with the keyboard. However, upon analysis of the log file, false triggers were flagged easily due to their characteristic closely-spaced timing. The task performed with the mouse required the button to be held for upwards of 100ms, and therefore false triggers were rare occurrences. Velocity measurements were difficult to ascertain due to the tendency to partially press

down the button in anticipation of the coming button press. As the velocity measurement was taken as an average velocity over the whole button press, depending on how the button was pressed, the velocity measurement was not always representative of the terminal velocity of the depressed button. If the finger was hovering just above the button before depressing it, the velocity could be measured with good repeatability and dynamic range. Due to the diffuse reflection off of the aluminium foil, the optical SNR was not as high as could have been achieved.

Mouse calibration

An attempt was made to optimize the tradeoff in setting the V_H and V_L reference thresholds to limit false triggering by separating the thresholds as far as possible while at the same time raising V_L toward V_H such that lightly resting a finger on the button before depressing it would not cause the state machine to rest in the “partially-depressed” state. Due to slight shifts in angles and sensitivities from one setup to another, recalibration was often required upon reconfiguration.

While real-time auditory feedback was not presented with the button pressing task, mapping the timing data to the seven-bit MIDI velocity range was not required. As well, due to the difficulty in constraining the way in which the button was pressed, which then impacted the accuracy of the velocity data, the velocity data could not be used as a reliable source of behavioural data, and though it was collected, was all but abandoned during analysis.

MR-compatibility

The mouse-like response box was used as a replacement for the commercial computer mouse that was functioning properly in the 1.5T scanner and which did not function properly when

the task was migrated to the $3T$ scanner. The MR-compatible response box detailed in this thesis functioned properly in the MR scanner, with no difference in performance from one environment to another. As of this writing, field homogeneity and scanner SNR tests have yet to be performed, though they are planned. Scanning with the device did not create any visible image artifacts in anatomical nor functional scans. A study performed by Christopher Steele employed the MR-compatible mouse to great effect and details are available in his Master's thesis [71]. The experiment studied the neural correlates of motor learning using a tapping task of non-standard musical rhythm. Mouse button presses were collected on a host computer and synchronized with the scanner and visual stimuli. The mouse performed successfully, allowing collection of behavioural data and functional scans without the scanner affecting the mouse, or vice versa.

Figure 5.5 shows functional MR images² taken on the coronal, axial, and sagittal planes respectively, during a rhythmic tapping task using the fMRI-compatible mouse. The task required that the subjects reproduce a timed sequence of button presses in synchrony with flashing visual stimuli, followed by a forty-second rest period. The sequence consisted of sets of long ($600ms$) and short ($300ms$) durations interlaced with a constant $300ms$ inter-stimulus interval. No feedback was presented. Scanning was done at the Montreal Neurological Institute's Brain Imaging Centre with images acquired using a Siemens $3T$ TRIO whole-body MRI scanner equipped with an eight-channel head coil and a T2*-weighted functional protocol ($4mm$ isotropic resolution; $2.5s$ relaxation time; $30ms$ echo time; $256mm$ field of view; 90 degree flip angle; 64×64 matrix).

²Courtesy of Christopher Steele, used with permission.

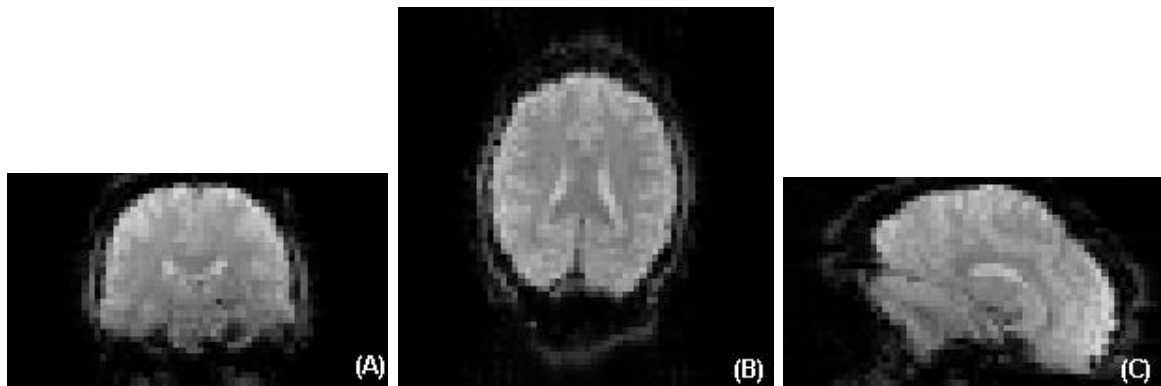


Fig. 5.5 Functional MRI scans with mouse.
(A) coronal, (B) axial, and (C) sagittal slices of a subject performing a rhythmic task with the fMRI-compatible mouse in the scanner.

5.2 Recommendations and future work

The interfaces presented above are but the first in a set of proposed MR-compatible musical controllers. Next generation prototypes are planned which will improve upon the ones already constructed. While proof of concept has been shown, and the feasibility of performing musical tasks with specialized devices proven, design changes can be made to improve functioning and robustness.

5.2.1 General recommendations

Starting with the circuitry, it is recommended that a printed circuit board be developed in order to take advantage of the surface-mount ICs with more pins and a smaller footprint. This would simplify board wiring, increase robustness, and enable many more input channels to be made available on a single PSoC package. Special considerations should be made to allow for in-circuit serial programming of the PSoC. Panel-mounting of optical connectors and terminating optical fibres with industry standard locking connectors would increase reliability and reduce time spent debugging and calibrating. Optical fibers need

to be properly cut and polished in order to achieve optimal signal transduction.

It is recommended that an autocalibration routine be implemented in firmware in order to improve performance and reduce setup time. The system would involve an analog-to-digital converter multiplexed for each input channel. Instead of manual trim potentiometers to set the threshold reference voltages, electronically-controlled potentiometers would be employed. As well, additional electronically-controlled potentiometers and circuitry would allow variable gain and offset adjustments for each channel. Conversely, a more powerful and higher speed microcontroller with onboard analog-to-digital converters could replace the PSoC and comparators. With this architecture, key press and release thresholding, accomplished in firmware, would be applied to the digitized signal.

Using a switch to enable the calibration mode when engaged, and an array of LEDs to denote which channel's key (or button in the case of the mouse) to depress, calibration would proceed by depressing and releasing the keys one at a time as prompted by the control circuitry. The key would be depressed multiple times with two or more MR-compatible reference weights, each corresponding to a different strike velocity. By lightly resting the weight atop the key and dropping it cleanly, each key should receive a uniform force for each weight. Multiple trials would be made for each key-weight configuration to ensure repeatability and to improve accuracy. The firmware routine, taking measurements of the key's sensor-weight profiles, would determine optimal parameter settings. In order to totally automate the calibration process, MR-compatible actuators on each channel would displace the key with a known position profile, setting the parameters to match the sensor data with the position data as closely as possible. The calibration process would optimize within-channel SNR to avoid false triggers and ensure key-to-key uniformity. This process is not limited to the keyboard, of course, but is applicable to the normalization of any sensor data originating from a set of nominally identical sources. As well, the key displace-

ment actuators could provide additional haptic feedback during device operation to render a more realistic feel, and could be used as another variable (or feedback modality) within neuropsychological imaging studies. By making use of the receive line of the communications module, the host computer can send commands to the interface control circuitry, enabling dynamic and adaptive operation.

5.2.2 Keyboard-specific recommendations

The main recommendation to improve the next generation keyboard prototype is to design the keybed and keys together with the sensing subsystem. Instead of mounting the sensors onto an already constructed keyboard, the optical subsystem should be integrated into the keyboard design from the very beginning to ensure optimal sensor alignment, key-to-key uniformity, and robustness. The mechanical specifications of the keyboard should conform to specified tolerances, and if need be, a means to make mechanical adjustments, as is available on acoustic pianos to allow for regulation, should be incorporated into the design. While increasing control over the setup of the device, along with the autocalibration scheme and locking optical connectors mentioned above, focus should be given to interface robustness and insensitivity to reconfiguration. Setup time should be reduced as much as possible, as time spent performing device calibration in the scanner is much more expensive than time spent at the design bench.

Work has already begun to design the next generation prototype with specially shaped keys to ensure proper key weighting and feel when played in a supine position to provide better ergonomics for finger and wrist angles. As well, a fixture is currently being developed in order to properly position and fix the keyboard above the subject while scanning, as shown in Figure 5.6.³ Special attention has been made to ensure the safety of the subject

³Courtesy of Brian Hynes, Hybex Innovations Inc, used with permission.

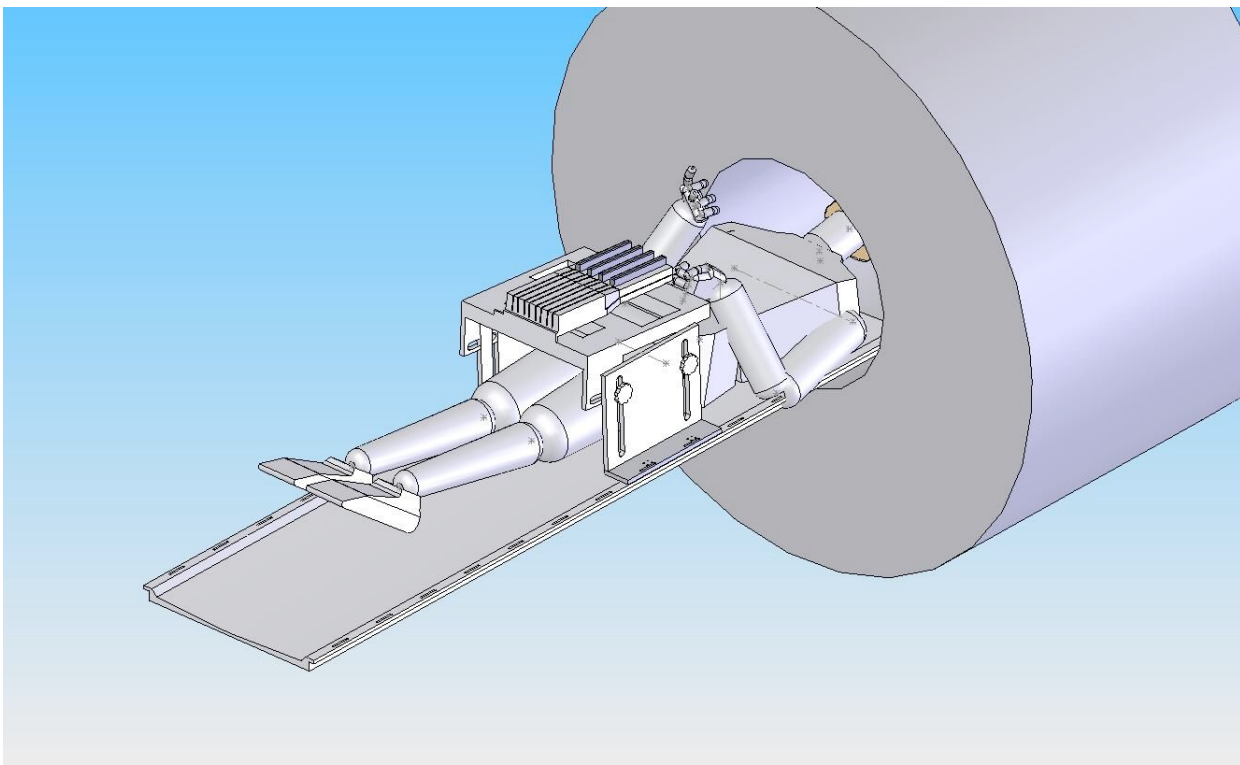


Fig. 5.6 Interface positioning fixture.

A computer-aided drawing of the conceived interface positioning fixture, showing a cut-away of the MR scanner with the keyboard fixed in position above the subject.

by including a method to quickly remove the interface in order to speedily extricate the subject in case of an emergency.

Isometric force sensing utilizing the transducer detailed in Section 4.3.3 and continuous position measurements using linear optical quadrature encoding should be pursued. If continuous position sensing is shown to be feasible, special attention during the mechanical design stages must be paid to ensure that the lever-like mechanism of the key is maintained such that the key does not lift at the balance point, as was discussed in Section 5.1.2. Upgrading the optical assembly with plano-convex focusing lenses on the reflector-side of the optical fibre has shown to significantly increase the optoelectronic SNR in laboratory tests, and should be considered for future generations of the prototype.

Onboard sound synthesis integrated into the interface electronics is another area to explore. While the implemented microcontroller is insufficient in terms of processing power to generate realistic real-time feedback, a co-processor optimized for sound synthesis coupled with a high quality digital-to-analog converter could provide improved auditory feedback without taxing the host computer.

5.2.3 Mouse-specific recommendations

Foremost, the replacement of diffuse reflectors with plane mirrors would improve the optoelectronic SNR, allowing better button press discrimination and more robust velocity measurement. While the foil reflector desensitizes the system to fibre alignment, variability in the amount of light reflected is exacerbated by deformations in the reflector surface. A plane mirror, though the alignment is crucial, provides a much more deterministic response and thus facilitates the measurement of button transition timing and velocity, easing calibration and setup time.

Starting with a computer mouse that has longer button travel and reduced contact point sensitivity would relax the interaction requirements and allow subjects to use the interface in a more comfortable manner. No longer would there be an obligation to tap gently on a specific part of the button. Longer button travel would physically isolate the released and depressed states, allowing the user to rest the finger on the button without it reporting the button in the “partially-depressed” state. While some computer mouse designs respond better to forces directed onto specific areas of the button, central to their functioning is that the haptic “click” of the mechanical switch corresponds directly to, and is synchronized with, the electronic communication of a signal denoting the press of the button. Wherewith indirect sensing, the fMRI-compatible response box attempted to provide the same feel and similar function, however next generation prototypes should expand the functionality to

general usage, ensuring the analogy.

5.3 Summary

In this chapter we discussed prototype testing, calibration, and *in situ* results, as well as made recommendations toward improving next generation interfaces. Proper device functioning was obtained after significant calibration, involving both systematic and subjective iterations. An autocalibration scheme was posited to decrease setup time. The piano keyboard suffered from key-to-key nonuniformities, while the mouse was hampered by short button travel and position-dependent force-to-displacement variations. Mechanical design improvements were suggested to alleviate these issues. The devices operated properly within the MR environment and caused no visible image artifacts.

Chapter 6

Conclusions

Overall the device prototypes performed successfully, showing the feasibility of conducting neuropsychological imaging experiments involving performance of musical tasks utilizing fMRI-compatible electronic musical interfaces. The devices developed as part of this project were designed to provide a physical interface for use by the subject inside the MR environment as part of a musical task. The devices measured subject interaction and transmitted behavioural data to a host computer for logging and synchronization with stimulus, feedback, and the imaging system itself. The MR environment presents many challenges to the proper functioning of an electronic device, due to intense and volatile electromagnetic fields. Not only are electronic devices sensitive to the fields within the MR environment, but the scanning apparatus is itself highly susceptible to interference from extrinsic sources, leading to degradation of image quality and artifact generation. Optical sensing and signal transmission within the MR environment is immune to electromagnetic interference, therefore photoelectronic sensing techniques were implemented using optical fibres. The devices were shown to be MR-compatible and function properly inside the scanner. Two devices were prototyped: a piano keyboard and a two-button response box in a computer mouse

form factor.

6.1 Summary of fMRI-compatible piano keyboard

For use in fMRI motor learning studies of piano playing tasks, the electronic keyboard was designed to emulate the feel of an acoustic piano. In order to capture behavioural data, a means to distinguish key presses and releases, as well as measure key strike velocity were incorporated into the interface. The keyboard prototype, built from part of an acoustic piano, was augmented with fibre optic sensors and stripped of all ferromagnetic parts. Due to the lack of a mechanical piano action and the age of the keyboard, the keys were re-weighted and re-felted to improve the feel. Calibration was needed to ensure the device functioned properly, as the trajectories of the depressed keys were not uniform. The device functioned successfully within the scanner, enabling real-time auditory feedback and logging of key presses.

Future fMRI-compatible keyboard prototypes should approach the design by incorporating the sensing system into the keyboard from the very beginning, instead of modifying an existing instrument. Tight tolerances and professional keyboard construction would ensure key-to-key uniformity, while electronic autocalibration would reduce setup time and increase device robustness. A movable fixture with a quick-release mechanism would allow the interface to be positioned in a customizable way, depending on subject size and comfort. As the subject performs with a supine posture, specially-shaped keys would further alleviate ergonomic concerns introduced by the scanner configuration. Key press force and key trajectory position profile should be studied as additional behavioural measurands.

6.2 Summary of fMRI-compatible computer mouse

A commercial computer mouse was being used for fMRI motor learning studies in a $1.5T$ scanner by neuropsychologists at the Montreal Neurological Institute. The experiment was migrated to a $3T$ scanner and the mouse no longer functioned properly because of the increased field strengths. Thus an MR-compatible computer mouse was designed to capture button press and release timing; translational information was not required. The form factor of this two-button response box was kept as a computer mouse to maintain a uniform feel across training sessions outside the scanner and testing sessions within. Fibre optic sensors mounted on the interface were connected to electronics in the control room outside the MR environment, allowing the collection and communication of button transitions and velocity. *In situ* manual calibration was required to ensure the device functioned properly, as button travel was minimal. Button presses were effected at specific sensitive locations of the mouse, marked by Velcro pads, which provided a tactile target area. The interface succeeded in reproducing the feel of a computer mouse, and button presses were sensed successfully within the MR environment during scanning sessions.

Future fMRI-compatible computer mouse prototypes should be insensitive to finger-button contact point and more robust against false triggers, by incorporating a mouse with longer button travel and non-diffuse reflectors. These design changes would also lead to improved measurement of transition velocity.

6.3 Future MR-compatible interfaces

It has been shown that optical sensing and signal conveyance can be successfully applied to MR-compatible interfaces. Optical sensing techniques, however, are sensitive to proper alignment of subsystem components. Mechanical shifts brought about by setup and tear-

down need to be minimized. While leaving a device set up in the scanner as a permanent installation is infeasible, as the scanner is used by many different parties for disparate purposes, device robustness to the resulting mechanical stress is central to proper operation with each successive use. As such, the design should include opto-mechanical connections that are reliable and provide repeatable results. Concurrently, autocalibration procedures incorporated into the design should ensure that any changes that do result between configurations are effectively nullified. Time taken performing manual calibration in the MR environment is inefficient and unnecessary. MR-compatible devices, be they for neuropsychological applications or not, can be augmented with MR-compatible sensors and actuators to create a closed-loop system for completely automated calibration. Additionally, actuators can enhance the haptic feedback of the device by reproducing forces that would normally be available to interfaces outside the MR environment, such as the mechanical piano action.

In addition to improving the designs of the piano keyboard and two-button response box, other fMRI-compatible devices are planned. The design of an MR-compatible *flute à bec* (recorder) and cello are planned. One has to remember that the MR environment is noisy and not conducive to audio acquisition. As well, it is the direct acquisition of subject-device interaction that is of primary concern in motor learning studies. The playability and realism of the emulations will depend on the task required, however many of the techniques discussed in this manuscript are applicable. Pitch selection through finger positioning can be optically sensed in a binary fashion as before, though variations in finger reflectivity will have to be circumvented. Optical force measurement has also been discussed previously, and will continue to be explored. Air and bow speed measurements can be accomplished in many different ways, with angular quadrature encoding perhaps being the simplest and most reliable. An extension of these techniques could lead to further advances in not

only fMRI-compatible musical instruments, but novel electronic musical instruments and innovative MR-compatible robotic interfaces as well.

Microfabrication of optical transducers on flexible substrates will do much to improve the accuracy and spatial resolution of MR-compatible sensors. The sensor packing density of force sensors, for instance, would allow for pressure profiles with sub-millimetre resolution. Not only would these types of sensors be useful for musical instruments (MR-compatible, or not), but they would also provide MR-compatible surgical robotic systems with the requisite sensing needed to provide the operator with analogous haptic feedback.

Continuous sensing of a larger number of inputs gives rise to much more data than simple transition information, and thus requires higher throughput capacity for data processing. Depending on the extent to which resources are encumbered, multiplexers, co-processors, and increased memory size may be required. Communication of behavioural data may be processed on-chip and sent as meta-information while more advanced communications protocols, such as OSC, should be explored.

6.4 An insight on electronic musical instrument design

In designing an electronic musical instrument, for use within the MR environment or without, sensing the musician's interaction with the instrument and translating those measurands into representative sounds is paramount. Equally important, though often overlooked, is the feel of the device [31, 32]. A dearth of haptic feedback brought about by contact-less sensing impedes elevated performance. It is posited that a novel instrument which provides a physical interface with movable or deformable parts (or a mechanical self-actuating response), replete with distributed sensing to measure the total physical interaction between the user and interface, and mapping that interaction onto a physical or physically inspired

dynamical model for sound synthesis, will begin to approach the playability and timbral nuance of acoustic instruments.

Embedded systems enable the design of specialized stand-alone devices, with sensing, control, and feedback systems operating in the absence of a personal computer. Without relying on a host computer running multiple layers of software, the instrument can function without latency and fear of crashes. Although, a means of connecting the device to a personal computer is encouraged for easy customization and tuning using a graphical user interface, migrating or sharing settings, and installing firmware updates.

Optical sensing is an affordable method for distributed sensing, providing high sensitivity and immunity to electromagnetic interference. Combined with mechanically-sound construction and an appropriate calibration scheme, a robust interface can be implemented. Though there have been attempts at such a feat in the past [64], some devices, such as the optoelectronic version of Donald Buchla's Thunder, never made it to market. Buchla was granted a patent on an optoelectronic system for detecting the deformation of a membrane for use in a musical instrument [8]. There are, however, significant improvements that can be made to his patent.¹ Although there have been attempts that seemingly failed to come to fruition, there are still many avenues to explore, and hedges to prune.

¹Described therein is a method and system for localizing and estimating the pressure of multiple deformations of a membrane. The proposed embodiments utilize nominally-aligned emitter and receiver pairs to sense the reflection off of the membrane, as well as light scattered to non-paired detectors through deformation of the membrane. An embodiment incorporating quadruples of closely-spaced detectors, arranged in a two-by-two grid, wherever the patent notes the placement of a single detector, would allow for two-dimensional differential sensing, and would much improve the sensitivity and accuracy of the system.

Appendices

Appendix A

An introduction to the physics behind functional MRI

Oxygenated hemoglobin is weakly diamagnetic, meaning it has a very small and negative magnetic moment under an applied external magnetic field, due to its slight negative susceptibility. The magnetic moment M_0 generated in a tissue sample is related to the externally applied magnetic field B_0 and its magnetic susceptibility χ :

$$M_0 = B_0\chi$$

Deoxygenated hemoglobin on the other hand is paramagnetic and thus has a small yet significant positive magnetic moment under an applied magnetic field. The changes in susceptibility between oxygenated and deoxygenated blood impact the local or microscopic magnetic field strength.¹

¹It should be noted, however, that because the hemoglobin makes up only a part of the red blood cell, and that red blood cells, in turn, make up only a part of the blood, the overall change in the blood's susceptibility is quite small though detectable with specialized equipment.

The first step toward generating a functional MR signal is to place the head of the patient within a strong magnetic field in order to reorient the normally randomly distributed magnetic dipoles of the hydrogen nuclei (as seen in Figure A.1 (A)) of the cerebral tissue so that they all point along the same axis (that is parallel or anti-parallel to the externally-applied B_0 field). A quantum mechanical effect is found when the H^+ species are placed in a magnetic field, which causes the magnetic dipoles to take on only one of two possible states or energy levels known as spin-up and spin-down, referring to the lower energy parallel alignment and higher energy anti-parallel alignment, respectively. The rest state of tissue containing a large population of protons has a net parallel-aligned magnetic moment and thus is the lower energy state, as shown in Figure A.1 (B). An excitation, through the addition of energy, will cause the spin-up particles to jump up to the higher energy state thus becoming spin-down protons, while the higher energy spin-down protons drop down to the lower energy state thus creating an overall higher energy state. Relaxation from this excited state can manifest in two ways: firstly through spin-lattice relaxation as the energy released by the protons as they jump to the low-energy state is absorbed by the molecular lattice structure; or secondly, relaxation may be in the spin-spin form whereby energy released by high-energy protons as the jump down to the low-energy state is transferred to the protons in the low-energy state causing them to jump into the higher-energy level. This process can continue for several iterations of self-excitation. The term jump is used as the action is not a gradual or continuous one, but a discrete quantum phenomenon.

The phenomenon of quantum spin is usually discussed in a simplified manner for explanations of nuclear magnetic resonance by falling back on classical theories of magnetic dipoles. Having aligned the the magnetic dipoles using an external magnetic field, we can excite the protons (hydrogen nuclei) and reorient their magnetic dipoles using an intense burst of electromagnetic radiation at a specific resonant frequency, known as the (angular)

Larmor frequency given by the equation:

$$\omega_0 = \gamma B_0$$

where w_0 is the Larmor frequency, γ is the gyromagnetic constant of the sample, and B_0 is the externally-applied magnetic field. It is interesting to note that the resonant frequency for a given sample increases with an increase in the applied magnetic field. For hydrogen, the most commonly-found species in the human body and the atom which produces the most prominent MR effect, this nominal frequency falls into the radio frequency (RF) range for a 3T scanner:

$$f_0 \approx 42.56 \frac{MHz}{T} \cdot 3T = 127.68 MHz$$

Due to local inhomogeneities in the magnetic field caused by applied gradient magnetic fields or changes in magnetic susceptibility (known as a chemical shift), the resonant frequency of hydrogen in tissues vary about this nominal value. Thus an excitation pulse centered at the nominal frequency, and having narrow yet significant spectral side lobes, will excite certain nuclei more than others. The momentary excitation of a proton is followed by a relaxation period, as the proton returns to its rest state, that is, as it aligns itself once more with the externally-applied magnetic field, as seen in Figure A.1 (C). The proton precesses like a dreidel until it falls back into alignment with the applied magnetic field, in so doing it emits a weak, yet measurable, electromagnetic signal. This process of excitation and MR signal transduction is carried out in an MRI scanner with an RF emitter antenna and a head-coil receiver antenna respectively. The gradient magnetic fields are generated using resistive electromagnets.

The fMRI signal is normally evoked using what is called a T2*-weighted pulse sequence. This is accomplished using a 90 degree pulse (i.e. one that flips the dipoles perpendicular

to the B_0 field) and measures the time taken for this bulk transverse magnetic moment to decrease to 37% of its initial value. If we were to look at one individual excited nucleus, the magnetic moment would precess about its axis at its resonant frequency first in the transverse plane and then gradually fall back into alignment with the B_0 field. We are measuring, however, the signal induced in the receiver coil at the macroscopic level, which takes in to account the net magnetic moment of many hydrogen nuclei at once. Even in ideal conditions with a completely homogeneous B_0 field, without applied gradient fields, the inhomogeneities in the local magnetic field will cause nearby nuclei to precess at slightly different frequencies, and so the dipoles which were originally precessing in phase begin to dephase, with a relative change in phase proportional to the difference in Larmor frequency. This dephasing causes the net magnetic moment to decrease more quickly than any individual nucleus' magnetic moment. Add to that the gradient magnetic fields and the inhomogeneities caused by imperfections in the B_0 field, and you have a relaxation time dependent on not only the nuclei themselves but magnetic field homogeneity from a variety of sources. It is for this reason that even the slightest aberration in magnetic field homogeneity within the scanning volume caused by an interface brought into the scanner will have a significant impact on the results.

Due to the fact that a precessing dipole emits energy at a frequency that depends on the applied magnetic field strength, if the head of a subject is placed in a spatial gradient magnetic field (i.e. a magnetic field with an increase in intensity as a function of distance along a spatial dimension), the emitted MR signal will therefore contain different frequency components, each corresponding to emissions at various positions along the subject in the direction of the gradient field. Electromagnets within the scanner are switched on and off throughout the scanning process, effectively focusing the imaging system to image successive cross-sections or slices. An image can be created from the MR signal by applying

an inverse Fourier transform: extracting the frequency-encoded spatial information from the MR signal.

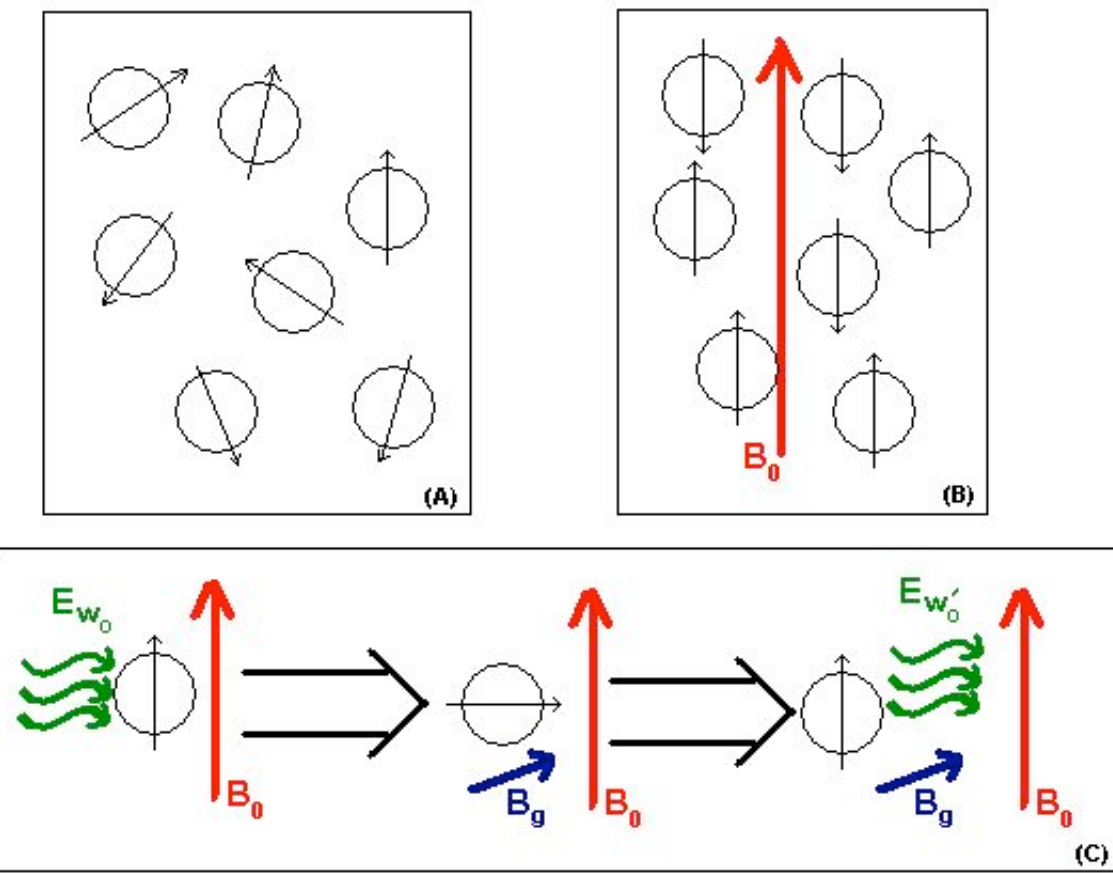


Fig. A.1 Magnetic resonance in action.

Figure (A) shows the magnetic dipoles with randomly distributed alignment without externally-applied magnetic field. Figure (B) shows dipoles aligned parallel and anti-parallel to the B_0 field, in a slightly net spin-up or low energy state. Figure (C) shows the time evolution as a single dipole (which can also represent the macroscopic model) aligned with the B_0 field absorbing an amount of RF energy, E_{ω_0} , at the sample's resonant frequency; having been excited by the 90° RF pulse, the dipole flips perpendicular to the B_0 field, meanwhile a gradient magnetic field, B_g , is applied; as the dipole relaxes and returns to its rest state, it emits an amount of energy $E_{\omega'_0}$, however due to B_g , the resonant frequency has shifted.

Appendix B

Forces due to magnetic fields exerted on ferromagnetic materials

The translational force exerted on an isotropic object (ellipsoid) by an external magnetic field B_0 is given by:

$$F_z = \frac{\chi V}{\mu_0} B_0 \frac{\partial B_0}{\partial z} \left[\frac{\cos^2 \theta}{1 + \chi D_a} + \frac{\sin^2 \theta}{1 + \chi D_r} \right]$$

where χ is the magnetic susceptibility, V is the object's volume, μ is the magnetic constant, θ is the angle between the object's axis of symmetry (the x-axis in this case) and B_0 , D_a and D_r are axial and radial demagnetization factors respectively [69]. Please refer to Table B.1 for demagnetization factors for various ellipsoid shapes. Even if a foreign object is already within the isocentre of the magnet, and thus will not become a projectile, torques may still exist due to its shape or anisotropic susceptibility that could reorient the ferrous object within the body causing anything from an odd, yet benign, sensation to untold harm or death. The torque exerted on an isotropic object (ellipsoid) by an external magnetic

field B_0 is given by:

$$T_y = \frac{\chi^2 V B_0^2}{\mu_0} \frac{(D_a - D_r)}{(1 + \chi D_a)(1 + \chi D_r)} \cos \theta \sin \theta$$

Therefore it is imperative that any device designed for the MR environment be free of ferromagnetic material. A caveat may include, however, that ferromagnetic objects that are properly secured and significantly far away from the scanner may not pose a threat, however their deployment in the MR environment should be avoided if at all possible and relegated to the control room.

	Sphere	Needle	Disk
D_a	$\frac{1}{3}$	0	1
D_r	$\frac{1}{3}$	$\frac{1}{2}$	0

Table B.1 Demagnetization factors for spherical, needle-like, and flat disk-like ellipsoids.

References

- [1] T. Ahn, S. Moon, Y. Youk, Y. Jung, K. Oh, and D. Kim. New optical frequency domain differential mode delay measurement method for a multimode optical fiber. *Optics Express*, 13:4005–4011, May 2005.
- [2] A. Askenfelt and E. V. Jansson. From touch to string vibrations. I: Timing in the grand piano action. *The Journal of the Acoustical Society of America*, 88:52–63, July 1990.
- [3] A. Askenfelt and E. V. Jansson. From touch to string vibrations. II: The motion of the key and hammer. *The Journal of the Acoustical Society of America*, 90:2383–2393, Nov. 1991.
- [4] M. Bangert, T. Peschel, G. Schlaug, M. Rotte, D. Drescher, H. Hinrichs, H.-J. Heinze, and E. Altenmuller. Shared networks for auditory and motor processing in professional pianists: Evidence from fMRI conjunction. *NeuroImage*, 30:917–926, Apr. 2006.
- [5] S. Baumann, S. Koeneke, M. Meyer, K. Lutz, and L. Jäncke. A network for sensory-motor integration: What happens in the auditory cortex during piano playing without acoustic feedback? *Ann NY Acad Sci*, 1060:186–188, Dec. 2005.
- [6] J. Berthold. Historical review of microbend fiber-optic sensors. *Journal of Lightwave Technology*, 13:1193–1199, 1995.
- [7] M. A. Brown and R. C. Semelka. *MRI: Basic Principles and Applications*. John Wiley & Sons, 3rd edition, 2003.
- [8] D. F. Buchla. System and method for detecting deformation of a membrane. Patent application, June 1999. United States Patent 5913260.
- [9] R. L. Buckner. Event-related fMRI and the hemodynamic response. *Human Brain Mapping*, 6:373–377, 1998.
- [10] Burdet, Gassert, Gowrishankar, Chapuis, and Bleuler. fMRI compatible haptic interfaces to investigate human motor control. *Experimental Robotics IX*, 21:25–34, 2006.

- [11] D. Chapuis, R. Gassert, L. Sache, E. Burdet, and H. Bleuler. Design of a simple MRI/fMRI compatible force/torque sensor. In *International Conference on Intelligent Robots and Systems*, volume 3, pages 2593–2599, 2004.
- [12] D. Chapuis, R. Gassert, E. Burdet, and H. Bleuler. Hybrid ultrasonic motor and electrorheological clutch system for MR-compatible haptic rendering. In *International Conference on Intelligent Robots and Systems*, pages 1553–1557, 2006.
- [13] D. Chapuis, X. Michel, R. Gassert, C.-M. Chew, E. Burdet, and H. Bleuler. A haptic knob with a hybrid ultrasonic motor and powder clutch actuator. In *EuroHaptics Conference and Symposium on Haptic Interfaces for Virtual Environment and Teleoperator Systems.*, pages 200–205, 2007.
- [14] E. Chen and B. Marcus. Force feedback for surgical simulation. *Proceedings of the IEEE*, 86:524–530, 1998.
- [15] J. L. Chen, R. J. Zatorre, and V. B. Penhune. Interactions between auditory and dorsal premotor cortex during synchronization to musical rhythms. *NeuroImage*, 32: 1771–1781, Oct. 2006.
- [16] K. Chinzei and K. Miller. Towards MRI guided surgical manipulator. *Medical Science Monitor*, 7:153–63, 2001. PMID: 11208513.
- [17] K. Chinzei, N. Hata, F. Jolesz, and R. Kikinis. Surgical assist robot for the active navigation in the intraoperative MRI: hardware design issues. In *International Conference on Intelligent Robots and Systems*, volume 1, pages 727–732, 2000.
- [18] Compaq Computer Corporation, Hewlett-Packard Company, Intel Corporation, Lucent Technologies Inc, Microsoft Corporation, NEC Corporation, Koninklijke Philips Electronics N.V. Universal serial bus specification. Technical report, USB Implementers Forum, Inc., 2000. Revision 2.0.
- [19] B. Culshaw. Optical fiber sensor technologies: opportunities and-perhaps-pitfalls. *Journal of Lightwave Technology*, 22:39–50, 2004.
- [20] Cypress Semiconductor. CY8C27143, CY8C27243, CY8C27443, CY8C27543, and CY8C27643 PSoC mixed-signal array final data sheet. Technical report, Cypress Semiconductor Corp., 2006. Available: http://download.cypress.com.edgesuite.net/design_resources/datasheets/contents/cy8c27443_8.pdf.
- [21] L. Danisch. Fiber optic bending and positioning sensor with selected curved light emission surfaces. Patent application, September 1995. United States Patent 5633494.
- [22] B. Deveaud, A. Quattropani, and P. Schwendimann. *Electron and photon confinement in semiconductor nanostructures*. IOS Press, 2003.

- [23] S. A. Finney. Auditory feedback and musical keyboard performance. *Music Perception*, 15(2):153–174, 1997.
- [24] M. Flueckiger, M. Bullo, D. Chapuis, R. Gassert, and Y. Perriard. fMRI compatible haptic interface actuated with traveling wave ultrasonic motor. In *Record of the 2005 Industry Applications Conference*, volume 3, pages 2075–2082, 2005.
- [25] N. Furstenau, H. Horack, and W. Schmidt. Extrinsic fabry-perot interferometer fiber-optic microphone. *IEEE Transactions on Instrumentation and Measurement*, 47:138–142, 1998.
- [26] G. Ganesh, R. Gassert, E. Burdet, and H. Bleuler. Dynamics and control of an MRI compatible master-slave system with hydrostatic transmission. In *IEEE International Conference on Robotics and Automation*, volume 2, pages 1288–1294, 2004.
- [27] R. Gassert, R. Moser, E. Burdet, and H. Bleuler. MRI/fMRI-compatible robotic system with force feedback for interaction with human motion. *IEEE/ASME Transactions on Mechatronics*, 11:216–224, 2006.
- [28] A. Gates, J. Bradshaw, and N. Nettleton. Effect of different delayed auditory feedback intervals on a music performance task. *Perception and Psychophysics*, 15(1):21–25, 1974.
- [29] Z. W. Geem, J. H. Kim, and G. Loganathan. A new heuristic optimization algorithm: Harmony search. *SIMULATION*, 76:60–68, Feb. 2001.
- [30] A. Giatti and M. Miniati, editors. *Acoustics and its Instruments*. Giunti, 2001.
- [31] B. Gillespie. *Music, Cognition, and Computerized Sound*, chapter 18: Haptics, pages 229–245. MIT Press, 2001.
- [32] B. Gillespie. *Music, Cognition, and Computerized Sound*, chapter 19: Haptics in Manipulation, pages 247–260. MIT Press, 2001.
- [33] W. Goebl, R. Bresin, and A. Galemba. Touch and temporal behavior of grand piano actions. *The Journal of the Acoustical Society of America*, 118:1154–1165, 2005.
- [34] S. Graham, W. Staines, A. Nelson, D. Plewes, and W. McIlroy. New devices to deliver somatosensory stimuli during functional MRI. *Magnetic Resonance in Medicine*, 46:436–442, 2001.
- [35] K. T. V. Grattan and B. T. Meggitt. *Optical Fiber Sensor Technology: Fundamentals*. Springer, 2000.

- [36] D. A. Hall, M. P. Haggard, M. A. Akeroyd, A. R. Palmer, A. Q. Summerfield, M. R. Elliott, E. M. Gurney, and R. W. Bowtell. Sparse temporal sampling in auditory fMRI. *Human Brain Mapping*, 7(3):213–223, May 1999.
- [37] R. J. Hanson, H. K. Macomber, A. C. Morrison, and M. A. Boucher. Primarily nonlinear effects observed in a driven asymmetrical vibrating wire. *The Journal of the Acoustical Society of America*, 117:400–412, 2005.
- [38] B. Haslinger, P. Erhard, E. Altenmuller, U. Schroeder, H. Boecker, and A. O. Ceballos-Baumann. Transmodal sensorimotor networks during action observation in professional pianists. *J. Cogn. Neurosci.*, 17:282–293, Feb. 2005.
- [39] M. C. Hirschkorn. Dynamic model of a piano action mechanism. Master’s thesis, University of Waterloo, Waterloo, ON, CA, 2004.
- [40] A. Hollinger, C. Steele, V. Penhune, R. Zatorre, and M. Wanderley. fMRI-compatible electronic controllers. In *Proceedings of the International Conference on New Interfaces for Musical Expression*, pages 246–249, New York, New York, 2007.
- [41] S. A. Huettel, J. D. Singerman, and G. McCarthy. The effects of aging upon the hemodynamic response measured by functional MRI. *NeuroImage*, 13:161–175, 2001.
- [42] A. Hunt, M. M. Wanderley, and M. Paradis. The importance of parameter mapping in electronic instrument design. In *Proceedings of the International Conference on New Interfaces for Musical Expression*, pages 1–6, Dublin, Ireland, 2002.
- [43] Industrial Fiber Optics. Plastic fiber optic photodarlington: IF-D93. Technical report, Industrial Fiber Optics Inc., 2006. Available: <http://i-fiberoptics.com/leds/IFD93.pdf>.
- [44] Industrial Fiber Optics. Plastic fiber optic super-bright LED: IF-E97. Technical report, Industrial Fiber Optics Inc., 2007. Available: <http://www.i-fiberoptics.com/leds/IFE97.pdf>.
- [45] R. D. Inkster. Touch pad using a non-electrical deformable pressure sensor. Patent application, November 2001. United States Patent 6788295.
- [46] K. Itoh, Y. Fujii, K. Suzuki, and T. Nakada. Asymmetry of parietal lobe activation during piano performance: a high field functional magnetic resonance imaging study. *Neuroscience Letters*, 309:41–44, 2001.
- [47] G. A. James, G. He, and Y. Liu. A full-size MRI-compatible keyboard response system. *NeuroImage*, 25:328–331, Mar. 2005.

- [48] L. Jäncke, S. Baumann, S. Koeneke, M. Meyer, B. Laeng, M. Peters, and K. Lutz. Neural control of playing a reversed piano : empirical evidence for an unusual cortical organization of musical functions. *Neuroreport*, 17:447–251, 2006.
- [49] A. Kersey, M. Davis, H. Patrick, M. LeBlanc, K. Koo, C. Askins, M. Putnam, and E. Friebele. Fiber grating sensors. *Journal of Lightwave Technology*, 15:1442–1463, 1997.
- [50] A. Khanicheh, A. Muto, C. Triantafyllou, B. Weinberg, L. Astrakas, A. Tzika, and C. Mavroidis. MR compatible ERF driven hand rehabilitation device. In *9th International Conference on Rehabilitation Robotics*, pages 7–12, 2005.
- [51] T. Krings, R. Töpper, H. Foltys, S. Erberich, R. Sparing, K. Willmes, and A. Thron. Cortical activation patterns during complex motor tasks in piano players and control subjects. a functional magnetic resonance imaging study. *Neuroscience letters*, 278:189–93, 2000. PMID: 10653025.
- [52] J. Ku, R. Mraz, N. Baker, K. K. Zakzanis, J. H. Lee, I. Y. Kim, S. I. Kim, and S. J. Graham. A data glove with tactile feedback for fMRI of virtual reality experiments. *Cyberpsychology & Behavior*, 6:497–508, Oct. 2003. PMID: 14583125.
- [53] S. A. Lange and Q. N. Nguyen. Cables and electrodes can burn patients during MRI. *Nursing*, 36:18, November 2006.
- [54] C. J. Limb and A. R. Braun. Neural substrates of spontaneous musical performance: An fMRI study of jazz improvisation. *PLoS ONE*, 3(2):1–9, Feb 2008.
- [55] M. Lotze, G. Scheler, H. R. Tan, C. Braun, and N. Birbaumer. The musician's brain: functional imaging of amateurs and professionals during performance and imagery. *NeuroImage*, 20(3):1817–1829, November 2003.
- [56] C. N. Ludman, T. G. Cooper, L. L. Ploutz-Snyder, E. J. Potchen, and R. A. Meyer. Force of voluntary exercise does not affect sensorimotor cortex activation as detected by functional MRI at 1.5T. *NMR in Biomedicine*, 9:228–232, 1996.
- [57] Maxim Integrated Products. +5V-powered, multichannel RS-232 drivers/receivers. Technical report, Maxim Integrated Products Inc., 2006. Available: <http://datasheets.maxim-ic.com/en/ds/MAX220-MAX249.pdf>.
- [58] D. W. McRobbie, E. A. Moore, M. J. Graves, and M. R. Prince. *MRI from Picture to Proton*. Cambridge University Press, 2nd edition, 2007.

- [59] I. Meister, T. Krings, H. Foltys, B. Boroojerdi, M. Müller, R. Töpper, and A. Thron. Effects of long-term practice and task complexity in musicians and nonmusicians performing simple and complex motor tasks: Implications for cortical motor organization. *Human Brain Mapping*, 25:345–352, Apr. 2005.
- [60] MIDI Manufacturers Association Incorporated. The technology of MIDI, 2008. Available: <http://www.midi.org/about-midi/abtmidi.shtml>.
- [61] C. Misas, F. M. Araujo, L. Ferreira, J. Santos, and J. Lopez-Higuera. Fiber bragg sensors interrogation based on carrier generation by modulating the coupling length of a wavelength-division multiplexer. *IEEE Journal of Selected Topics in Quantum Electronics*, 6:750–755, 2000.
- [62] D. G. Mitchell and M. S. Cohen. *MRI Principles*. Saunders, 2nd edition, 2004.
- [63] R. Moretti, P. Torre, R. M. Antonello, M. Ukmar, R. Longo, and A. Bava. Learned movements in a left-handed pianist: an fMRI evaluation. *Journal of Clinical Neuroscience*, 9:680–4, Nov. 2002. PMID: 12604284.
- [64] J. Paradiso. Electronic music: new ways to play. *IEEE Spectrum*, 34:18–30, 1997.
- [65] V. B. Penhune, R. J. Zatorre, and W. H. Feindel. The role of auditory cortex in retention of rhythmic patterns as studied in patients with temporal lobe removals including heschl's gyrus. *Neuropsychologia*, 37:315–31, Mar. 1999. PMID: 10199645.
- [66] S. O. Pfleiderer, J. R. Reichenbach, T. Azhari, C. Marx, A. Malich, A. Schneider, J. Vagner, H. Fischer, and W. A. Kaiser. A manipulator system for 14-gauge large core breast biopsies inside a high-field whole-body MR scanner. *Journal of Magnetic Resonance Imaging*, 17:493–498, 2003.
- [67] R. Riener, T. Villgrattner, R. Kleiser, T. Nef, and S. Kollias. fMRI-compatible electromagnetic haptic interface. In *27th Annual International Conference of the Engineering in Medicine and Biology Society*, pages 7024–7027, 2005.
- [68] M. O. Scully and M. S. Zubairy. *Quantum Optics*. Cambridge University Press, 1997.
- [69] F. G. Shellock, editor. *Magnetic Resonance Procedures: Health Effects and Safety*. CRC Press, 2001.
- [70] C. J. Steele. Personal communications regarding non-fMRI-compatible computer mouse. Montreal, QC, CA, September 2006.
- [71] C. J. Steele. Tides of change: Identifying the neural correlates of motor sequence learning. Master's thesis, Concordia University, Montreal, QC, CA, November 2007.

- [72] C. E. Strangio. The RS232 standard: A tutorial with signal names and definitions, 2006. Available: http://www.camiresearch.com/Data_Com_Basics/RS232-standard.html.
- [73] M. Tada, S. Sasaki, and T. Ogasawara. Development of an optical 2-axis force sensor usable in MRI environments. *Proceedings of IEEE Sensors*, 2:984–989, 2002.
- [74] N. Takahashi, M. Tada, J. Ueda, Y. Matsumoto, and T. Ogasawara. An optical 6-axis force sensor for brain function analysis using fMRI. In *Proceedings of IEEE Sensors*, volume 1, pages 253–258, 2003.
- [75] M. Tremblay, F. Tam, S. J. Graham, and J. Kucharczyk. Optical image-based position tracking for magnetic resonance imaging. Patent application, April 2005. European Patent EP1524626.
- [76] H. S. Tzou and C.-S. Chou. Nonlinear opto-electromechanics and photodeformation of optical actuators. *Smart Materials and Structures*, 5:230–235, 1996.
- [77] F. T. Ulaby. *Fundamentals of Applied Electromagnetics*. Pearson Prentice Hall, 2004.
- [78] S. Urich. Dual 1000um plastic fiber optic cable. Technical report, Amp Inc., 2002. Available: <http://rocky.digikey.com/weblib/Amp/Web%20Data/501336.pdf>.
- [79] U.S. Food and Drug Administration: Centre for Devices and Radiological Health. MRI safety, September 2001.
- [80] J. Vogan, A. Wingert, J.-S. Plante, S. Dubowsky, M. Hafez, D. Kacher, and F. Jolesz. Manipulation in MRI devices using electrostrictive polymer actuators: with an application to reconfigurable imaging coils. In *IEEE International Conference on Robotics and Automation*, volume 3, pages 2498–2504, 2004.
- [81] M. Wright. The open sound control 1.0 specification, 2002. Available: http://opensoundcontrol.org/spec-1_0.
- [82] A. Yamamoto, K. Ichiiyanagi, T. Higuchi, H. Imamizu, R. Gassert, M. Ingold, L. Sache, and H. Bleuler. Evaluation of MR-compatibility of electrostatic linear motor. In *Proceedings of the IEEE International Conference on Robotics and Automation*, pages 3658–3663, 2005.
- [83] F. T. S. Yu and S. Yin. *Fiber Optic Sensors*. CRC Press, 2002.
- [84] L. A. Zaremba. Criteria for significant risk investigations of magnetic resonance diagnostic devices. Technical report, U.S. Department of Health and Human Services Food and Drug Administration Center for Devices and Radiological Health, 2003.